https://doi.org/10.1007/s11629-025-9925-4

Original Article | Collection on Advances in Sediment Connectivity and Sediment Dynamics Assessments for Mountain Geohazard Management

Optimising the identification of river sediment supply areas and their connectivity in the mountainous river basins of central Italy

GUIDI Erica[1*] https://orcid.org/0009-0003-7519-0996; e-mail: e.guidi16@campus.uniurb.it; ericaguidi95@gmail.com

PAPPAFICO Giulio Fabrizio[1] https://orcid.org/0009-0001-4683-4460; e-mail: giulio.pappafico@uniurb.it

CONFUORTO Pierluigi[2] https://orcid.org/0000-0003-4291-4604; e-mail: pierluigi.confuorto@unifi.it

MORELLI Stefano[1] https://orcid.org/0000-0001-8069-3609; e-mail: stefano.morelli@uniurb.it

* *Corresponding author*

1 Department of Pure and Applied Sciences (DiSPeA), University of Urbino 'Carlo Bo', Via Ca' Le Suore, 2-4, Urbino, Italy

2 Earth Science Department, University of Florence, Via La Pira 4, 50121 Florence, Italy

Citation: Guidi E, Pappafico GF, Confuorto P, et al. (2026) Optimising the identification of river sediment supply areas and their connectivity in the mountainous river basins of central Italy. Journal of Mountain Science 23. https://doi.org/10.1007/s11629-025-9925-4

Abstract: Climate change is increasingly exposing Mediterranean regions to extreme weather events with severe geomorphic impacts, such as flash floods, debris flows, and rapid landslides. Understanding the processes that supply sediment to catchment areas is crucial, given the strong upstream–downstream connectivity typical of mountainous regions. This can exacerbate vulnerabilities, cause localised flooding, and pose significant hazards. This study presents a semi-quantitative GIS-based procedure for optimising the identification of sediment supply areas and their structural connectivity in mountainous catchments of central Italy. The method combines three morphometric indices - the Stream Power Index (SPI), Index of Connectivity (IC), and Stream Length-Gradient (SL) index - derived from a detailed geomorphological characterisation of the study area. The methodology is designed to delineate sediment-source areas and assess their degree of connectivity with the drainage network. It incorporates a linear morpho-hydraulic component, based on SL index and longitudinal profile analyses, which supports the interpretation of channel energy conditions and sediment transfer dynamics. Finally, a synoptic raster map is generated to visually and spatially highlight the most critical values of the three indices. The approach was tested in the mountain portion of the Burano River basin (Northern Apennines), severely affected by the 15 September 2022 flood. The analysis revealed strong correspondence between high-connectivity areas and zones of post-event instability, indicating effective identification of both sediment sources and preferential transport corridors. Validation was performed through multi-source comparison, integrating Normalised Difference Vegetation Index (NDVI) analysis, UAV photogrammetry, and detailed traditional field surveys, thereby confirming the robustness of the results. The proposed approach is time- and cost-efficient and provides reliable insight into sediment transfer along slopes and river channels within a simplified and operational framework.

Keywords: GIS analysis; Sediment supply assessment; Catchment-scale sediment connectivity; Quick analysis procedure

Received: 26-Jun-2025
1st Revision: 09-Aug-2025
2nd Revision: 14-Nov-2025
Accepted: 12-Jan-2026

1 Introduction

Sediment transfer in mountainous basins plays a fundamental role in landscape evolution, water quality, and natural hazard dynamics, influencing the frequency and magnitude of floods, debris flows, and other slope instabilities (Harvey 2001; Fryirs 2013; Bracken et al. 2015), as well as the sediment balance within the river networks (Sadeghi et al. 2017; Liu et al. 2018). Although sediment mobilisation and transfer are inherently natural phenomena, they have been significantly modified by human activities, including land-use change, river regulation, and sediment trapping by dams and infrastructure, leading to accelerated erosion (Syvitski et al. 2005; Kemp et al. 2020). Understanding how sediments are mobilised and transferred through a catchment is essential to support risk mitigation and watershed management strategies (Fryirs 2017; Wohl et al. 2019). In this framework, the concept of sediment connectivity has emerged as a key tool to describe the degree to which a system facilitates or impedes sediment transfer between sources, pathways, and sinks (Brierley et al. 2006; Cavalli et al. 2013; Heckmann et al. 2018; Najafi et al. 2021a).

The International Sediment Initiative (ISI) was launched in 2002 by UNESCO's International Hydrological Programme (IHP) to promote sustainable sediment management globally (Liu et al. 2018). It aims to understand erosion and sediment transport by rivers to marine, lake or reservoir environments, aid in creating a decision-making framework for sediment management, and link science with policy and management needs. This framework offers guidance on legislative and institutional solutions applicable across diverse socio-economic and physiographic contexts under global change. In 2021, the Strategic Plan for the ninth phase of the IHP, titled "Science for a Water Secure World in a Changing Environment", was adopted by UNESCO in relation to the 2022 - 2029 period (Raphael et al. 2023). This phase identifies priority areas in support of Member States to achieve the Sustainable Development Goals (SDGs), focusing on the United Nations 2030 Sustainable Development Agenda and other water-related global agendas, such as the “Paris Agreement on climate change”, the increase “Sendai Framework on Disaster Risk Reduction” and the “New Urban Agenda” (UNESCO 2022).

The importance of understanding these phenomena is becoming increasingly evident, such as the concept of sediment production and its subsequent transfer to all potential minor collection basins. Considering the current increase in the intensity of rainfall events (Senatore et al. 2025), it is necessary to have rapid and practical responses, aligning with the objectives of global shared agendas. The assessment based on connection-disconnection hypotheses between slopes and the canal network (relationship between hillside slope and sediment transport; Bracken et al. 2015) is a comprehensive and innovative tool for analysing the system.

Over the past decade, research on sediment production and river connectivity has expanded considerably (Parsons et al. 2015; Wohl 2017; La Licata et al. 2025), with particular emphasis on hillslope–channel coupling. Within this framework, sediment connectivity is commonly described in terms of longitudinal connectivity, referring to coupling along the channel network, and lateral connectivity, referring to hillslope–channel interactions. Moreover, connectivity can be conceptualised as comprising two complementary components: structural connectivity and functional connectivity (Wainwright et al. 2011; Shi et al. 2025). Structural connectivity describes the spatial arrangement and geometric relationships among landscape elements, whereas functional connectivity refers to the actual transfer of sediment driven by hydrological and geomorphic processes, which varies in time in response to external forcing such as precipitation characteristics and antecedent conditions (Turnbull et al. 2018; Zanandrea et al. 2021). Although distinct, these two components are closely interrelated, as sediment transport can modify landforms and, in turn, alter structural pathways (Wohl et al. 2019). Given its static nature, structural sediment connectivity was the first to be quantitatively analysed using numerical and GIS-based models (Cavalli et al. 2013; Messenzehl et al. 2014; Cossart and Fressard 2017; Martini et al. 2022).

In particular, the river sediment connectivity was explored through i) assessment of the status of river sections, distinguishing between unconnected, partially connected, potentially connected, connected and disconnected areas (Hooke 2003). “Unconnected systems” refer to localised sediment sources and budgets in which individual reaches operate largely independently, whereas “disconnected systems” are those in which barriers such as dams or weirs have been constructed, preventing the downstream transfer

of coarse sediment over the lifetime of the structure; ii) analysis of the complex mechanisms involved in small- and large-scale sediment transport (Bracken et al. 2015); iii) development of approaches for morphological analysis using quantitative methods (Najafi et al. 2021a; Koreňová et al. 2024; La Licata et al. 2025); iv) development of morphometric indices (Mishra et al. 2019); v) introducing of new concepts such as (dis)connectivity in geomorphology associated with river and watershed management aspects (Poeppl et al. 2023).

According to Najafi et al. (2021b), who analysed 117 papers about the sediment connectivity, the problem is usually addressed from five points of view that are based on: i) developing conceptual frameworks; ii) depicting spatial and temporal distribution of sediment source and sink areas (morphological approach); iii) developing sediment connectivity indices (geomorphometric modelling); iv) using and developing models (based on existing or new software); v) investigating sediment delivery likelihood through a network analysis approach. Over 50% of the reviewed literature in Najafi et al. (2021b) calculates connectivity indices, with the Index of connectivity proposed by Borselli et al. (2008) and its subsequent modifications being the most widely adopted, as reported by Shi et al. (2025). Approximately one-fifth of the studies employ morphological approaches, while alternative methods are less commonly applied. Similar studies have begun to address the explicit link between erosion and sediment connectivity and to understand how geomorphological processes are fundamental to accurately estimating the sediment yield of a river basin. More recently, La Licata et al. (2025) introduced a model (named HOSTED) that clearly and explicitly integrates all the above-mentioned components, delivering as output a single and comprehensive raster map. This GIS-based model was designed for assessing potential hotspots of sediment dynamics at the watershed scale, integrating geomorphic spatial information with both structural and functional properties of connectivity.

Traditionally, studies of structural sediment connectivity conducted in GIS environments have relied primarily on the comparison of multiple, independent outputs derived from morphometric indices (Hooke & Souza 2021) without a truly coordinated use. In this work, a semi-quantitative GIS-based procedure is proposed that advances this approach by integrating, explicitly and structurally, those morphometric indices that prove most effective for describing connectivity across different parts of a basin. The framework aims to provide a coherent basis for optically identifying sediment-source areas, assessing their actual linkage to the drainage network, and interpreting the fate of sediment once it enters the channel; as well as a platform that can be readily integrated with functional indices for subsequent modelling. The procedure combines three key morphometric indices - the Stream Power Index (SPI; Abu El-Magd et al. 2021; Chowdhury 2023), the Index of Connectivity (IC; Cavalli et al. 2013), and the Stream Length–Gradient (SL) Index (Troiani et al. 2014) - derived from the geomorphological characterisation of the study area. Therefore, it is first specifically designed to identify sediment-supply areas and to evaluate their degree of coupling with the drainage network. Moreover, by explicitly incorporating a linear morpho-hydraulic component (SL and longitudinal-profile analysis), the method supports the interpretation of in-channel energy conditions and sediment-transfer processes.

The proposed method was developed and tested in a 92 km² hydrographic basin of the Northern Apennines (Italy), which was severely affected by the 15 September 2022 exceptional rainfall event. This remarkable occurrence triggered numerous landslides, widespread hillslope erosion, and severe flooding in the valley floors. The transfer of material between the slopes and the river networks was intense and complex due to the mountainous conformation of the area and the varied geological composition. Thanks to the geomorphic imprints left by these disruptions, the development of the approach benefited from the comparison between pre- and post-event datasets. A pre-event digital terrain model (DTM) was used to reconstruct the conditions prior to the flood, while the features preserved on the ground were employed to test the reliability of the proposed method. In addition, the availability of high-resolution post-event data allowed the validation to be carried out with a high level of accuracy.

2 Study Area

2.1 Geographical and climatic characteristics

The study area is located in the Northern Umbria-Marche Apennines (Central Italy), close to the

boundary between the Umbria and Marche regions at about 50 km from the Adriatic coast (Fig. 1). This is a predominantly mountainous sector of the Marche Apennines, whose slopes decrease eastward toward the Adriatic coastline to turn into hills that gently decrease towards the littoral zone. The most imposing relief is the Catria mount (1701 m a.s.l.; Fig. 2), part of a complex structure of almost parallel orographic lineaments in the N/NW-S/SE direction. The climatic characteristics of the area are influenced by exposure to the Adriatic Sea to the east and by the presence of the Apennines to the west, which obstruct the course of the western atmospheric currents, predominant in the local latitudes (Amici and Spina 2002). Distance from the sea, altitude, morphology, and exposure of the valley slopes are the most important geographical factors that define the climatic conditions. However, there may be variations in trends due to local influences. The climate of the study area can be classified as Mediterranean along the coastal zones, characterised by mild winters and hot summers. As elevation increases toward the Apennines, the climate transitions progressively toward continental conditions—with greater temperature swings and increased cold during winter months (Soldini and Darvini 2025). In the low hills and intermediate terrain between the coast and the mountains, the climate exhibits traits of sub-Mediterranean transitional zones, reflecting gradual changes in temperature, precipitation, and daily range across the east-west gradient (Soldini and Darvini 2025). According to Köppen's classification system (Köppen 1936), the territory is classified as having a moderate climate (class C). In particular, the climate can be identified with the sub-category Cfb (Latini 2018), which is characterised by average annual temperatures varying between 13° and 10°, a temperature range that reaches 14°-15°, and annual rainfall that oscillates between 1,000 and 1,500 mm. From the rain gauge close to the Catria mount, an average annual rainfall of 1,291 mm has been estimated from the available data from 1951 to 2024 (Regione Marche 2022).

From a hydrographic point of view, the rivers flow from west to east, with the Metauro being the longest

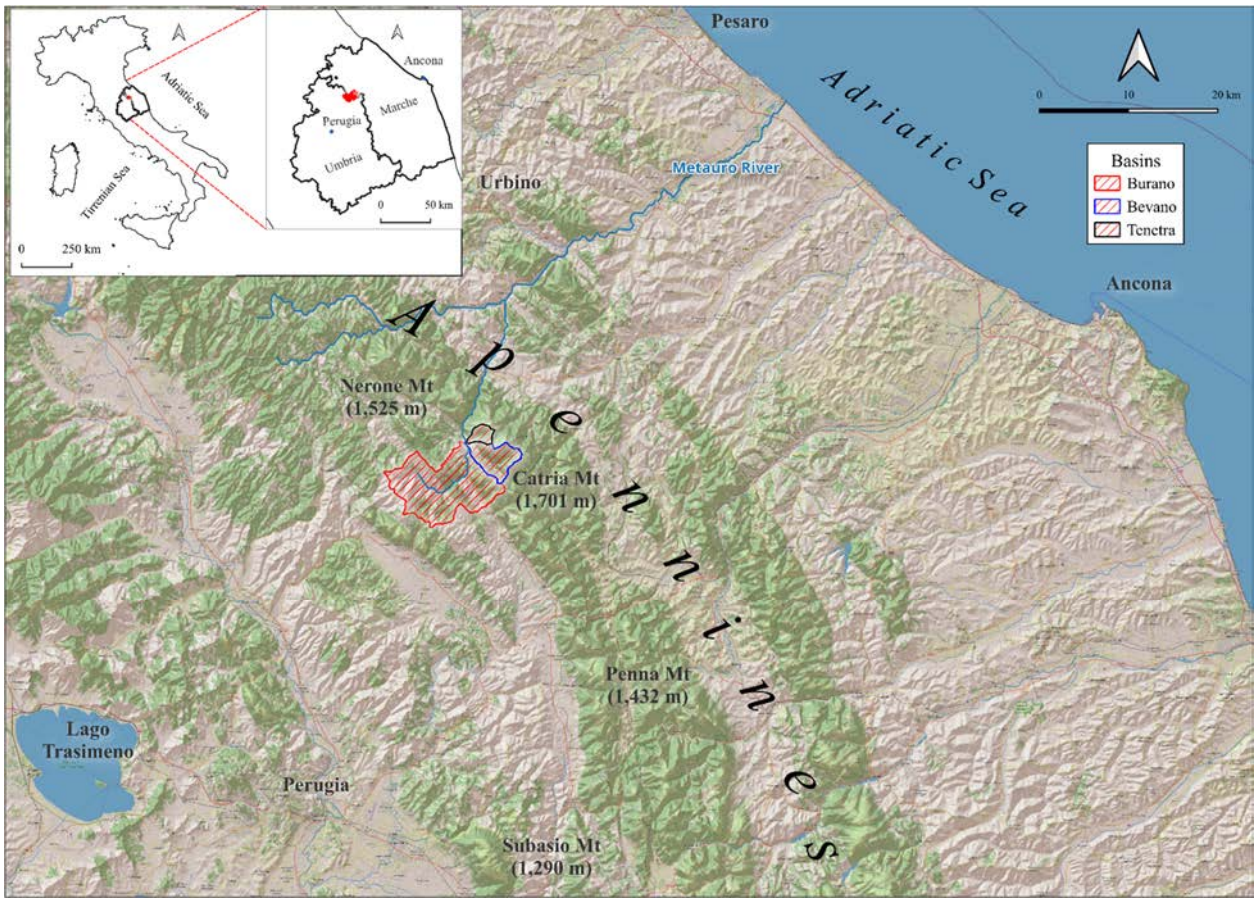

Fig. 1 Geographical location of the study area in the inner sector of the Northern Apennine Range. The three sub-basins are marked with differently coloured boundaries.

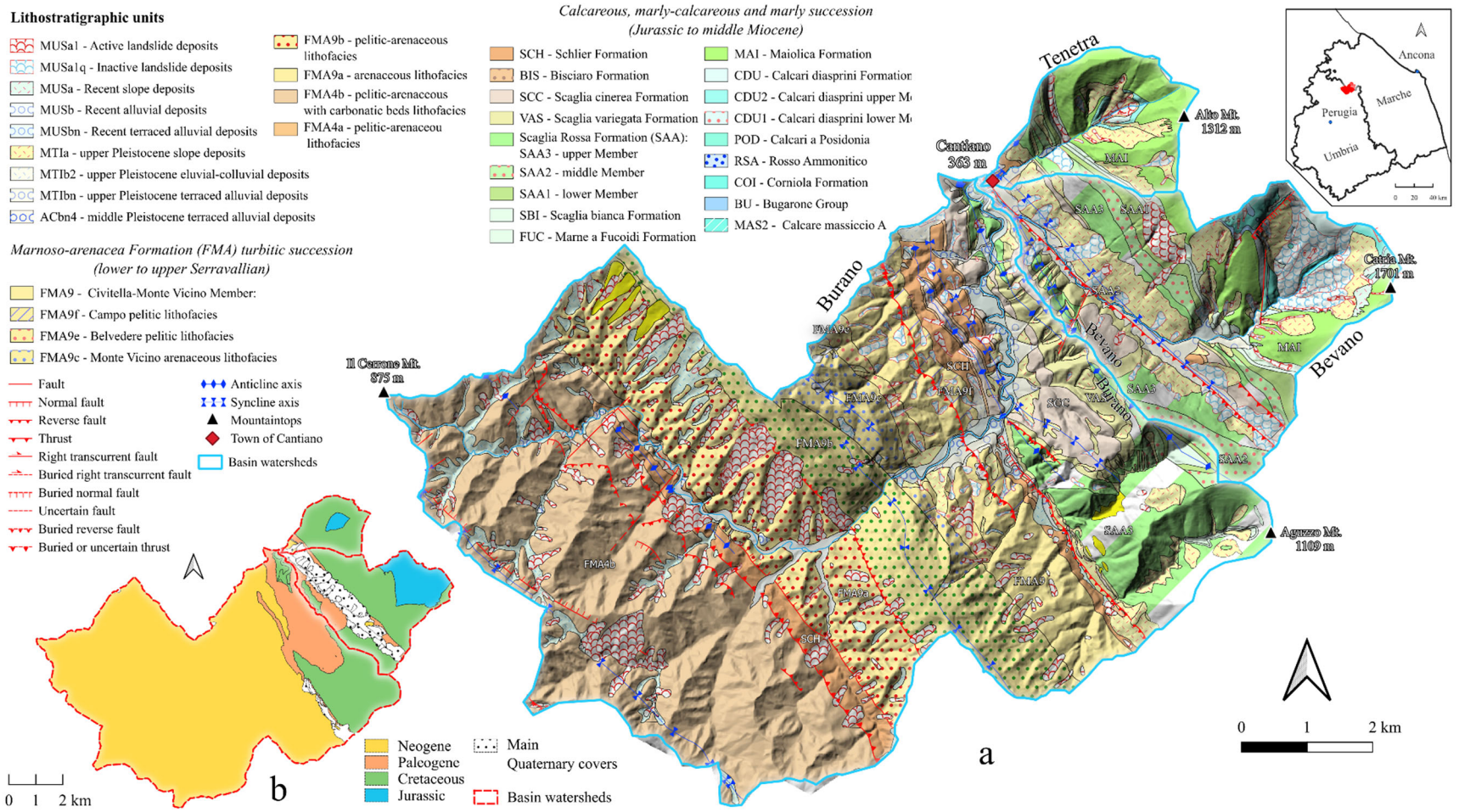

Fig. 2 (a) Geological map with the lithostratigraphic units derived from the official Regional Geological Cartography of Marche and Umbria regions (1996-2003); (b) Synthetic geological scheme highlighting the differences in type and age of the lithologies between the two north-eastern basins of Bevano and Tenetra, containing Jurassic-to-Paleogene carbonate-marl units, and the more extended Burano basin containing predominantly Neogene siliciclastic-terrigenous units.

river (121 km) (Gentilucci et al. 2020). The study area chosen for this research includes the upstream part of the Burano basin, whose closing section is located downstream of the built-up area of Cantiano. Before the end of the study area, there are two points where the main tributaries of the Burano converge, the Bevano and Tenetra streams, which cross the underground of the historic centre. Since these three sub-basins have different hydrological responses and different effects on the territory, their main characteristics are sometimes considered separately and compared throughout this paper (Fig. 1).

2.2 Geological setting

The study area is part of the Northern Apennines, a northeast-verging fold-and-thrust belt (Scisciani 2009; Barchi et al. 2012). The outcropping lithological units in the investigated area belong to the Umbria-Marche succession and span a time interval from the Jurassic to the middle-upper part of the Neogene (Fig. 2). The westernmost Burano basin differs from the Bevano and Tenetra basins in terms of the type and age of the outcropping lithostratigraphic units.

They also have different areal extents, the largest of which (Burano) includes predominantly Neogene siliciclastic-terrigenous units and a less extensive eastern portion adjacent to the other two basins, characterised by Cretaceous-to-Paleogene carbonate-marl units. The other two, less extensive river basins include Jurassic-to-Paleogene exclusively carbonate-marl lithostratigraphic units (Fig. 2b).

The different lithological characteristics of the upper Burano basin and its two tributaries make some of them more prone to producing material. In particular, the upper part of the Burano, upstream of Cantiano town, and the transition zones between one basin and another present rocks with a higher degree of erosion, which tend to disintegrate into very fine grains similar to sand and/or silt. In this area, landslides have often been attributed to the debris flow landslide type. On the contrary, the two secondary basins, located at the foot of the main anticline, are much more coherent and exhibit low degrees of erosion. They mainly produce sediment through rockfall processes or as a consequence of the erosion associated with large volumes of water flow. In the Tenetra basin, the highly erodible marnous unit of the “Marne a Fucoidi” formation outcrops, which produces sediments comparable to flattened pebbles. A large landslide with a significant accumulation at the base has formed on this channel, which was already present before the event. This paragraph does not take into account the deposits present before the event, but only the type of lithological composition.

This is reflected in the geomorphology of the territory, characterised by generally steeper slopes and more significant height differences in the two smaller basins compared to those of the larger basin (for more details, see section 4.1). Further, the distribution and areal proportion of the landslide types surveyed after the 15 September 2022 extreme event (Santangelo et al. 2023) seem to depend on the lithotypes occurring in the three basins and the type of slope detritus, which is abundant where predominantly carbonate terms crop out.

The lithological units are intensely fractured and contribute to the development, within the hydrographic basin system, of a dual-circuit groundwater network, which sustains baseflow even during dry periods. Structural lineaments trending NW–SE and SW–NE exert a strong control on both surface and subsurface hydrological dynamics, influencing the distribution of the springs and the orientation of the drainage network (Nanni and Vivalda 2009). The combination of steep slopes, lithological variability, and tectonic complexity results in a highly sensitive landscape to geomorphological processes such as erosion, shallow landslides, and fluvial adjustments.

2.3 The 15-16 September 2022 pluviometric event

On the evening of 15 September, a V-shaped, stationary and self-regenerating thunderstorm was formed in the Apennine chain of central Italy from storm cells originating on the Tyrrhenian side of the peninsula after becoming loaded with moisture during their path. Such a physical condition originated from a warm, humid mass of air moving from North Africa, with the simultaneous development of air convective systems favoured by the presence of humidity coming from the Tyrrhenian Sea and by the orography of the peninsula and its largest islands (Morelli et al. 2023). The event led to high precipitation amounts in a very short time (Table 1). It resulted in widespread criticality in the mountain areas of the basins on the eastern slopes of the Apennine chain and along some main courses up to their mouth (Fig. 3). The highest

Table 1 Cumulative rainfall in mm of the 15th-16th Sep 2022 event, measured by rain gauges of 9 stations located in the basins affected by the rainfall event: maximum measurements at 1, 3, 6, 12 and 24 hours (Regione Marche 2022). For the Cantiano rain gauge, the average intensity and the long-term average trend defined by the historical series of 71 years of records are shown.

Rain Gauge	Basin	Rainfall amount	1 h	3 h	6 h	12 h	24 h
Cantiano	Burano	Cumulative rainfall	101.4	256.6	384	419	419
		Average intensity in the hour interval (mm/H)	101.4	85.5	64.o	34.9	17.5
		Long-term average	26.5	37.7	8.8	66.6	88.7
Monte Acuto	Cesano	Cumulative rainfall	107.2	248.4	343.0	384.2	384.4
Arcevia	Misa	Cumulative rainfall	47.0	94.8	117.8	128.8	129.2
Barbara	Misa	Cumulative rainfall	50.8	111.4	121.2	127.0	127.2
Colle	Misa	Cumulative rainfall	77.4	162.4	186.4	204.0	204.0
Sassoferrato	Sentino	Cumulative rainfall	-	62.8	99.8	99.8	100.4
Colleponi	Sentino	Cumulative rainfall	42.4	68.0	122.0	122.2	122.6
Monte San Vicino	Musone-Esino	Cumulative rainfall	65.8	108.2	120.0	192.8	193.6
Cingoli	Musone	Cumulative rainfall	93.6	160.4	184.6	247.2	247.6

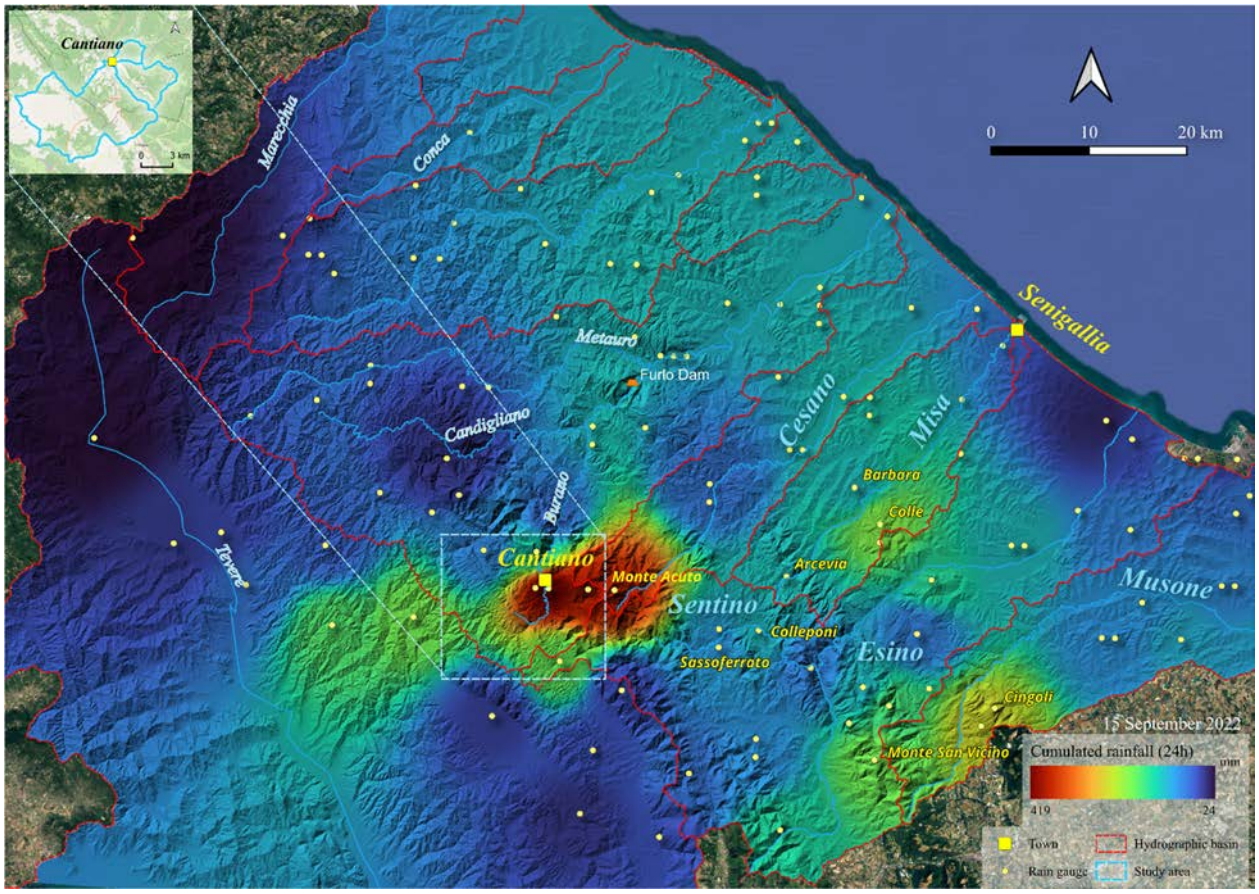

Fig. 3 September 2022 rainfall distribution concerning the main watercourses and related hydrographic basins. The position of the two most affected urban areas is highlighted (Senigallia is the most affected city in the plain area by the flood wave coming from upstream).

cumulated rainfall value was recorded at the rain gauge of Cantiano, with 419 mm in 12 hours (Table 1; Donnini et al. 2023), resulting in one of the most conspicuous events in the recording history of this area. Then, in the subsequent transit towards the coastal sectors of the Adriatic Sea, the storm system gradually weakened, losing intensity and progressively depleting. The pluviometric event covered a total area of 5,000 km^2 (Santangelo et al. 2023).

Table 1 summarises rainfall data recorded by rain gauges across the Marche region.t. The first three rows are associated with the Cantiano sensor and therefore

refer to the Burano Basin, the river under consideration. The first row shows the millimetres of water measured, the second the intensity in mm/h and the last one the long-term average trend defined by the historical series of this station. There are no other sensors, and these data are considered valid for the Burano basin upstream of Cantiano and for the two minor tributaries that flow into it laterally. Below the rows defining the values for Cantiano, we find a comparison with other rain gauges that recorded the same event in different river basins. The Misa and Cesano rivers suffered extensive damage as a result of the same extreme event.

Before the thunderstorm, the soil was substantially dry after a long summer drought. Rainfall network data show no significant precipitation within the 30 days before the event. Only about 61.4 mm cumulative between August 15 and September 1, and just a few mm in the first 15 days of September, were recorded from the pluviometer of Cantiano (RT-2972) of the Civil Protection Marche.

The combination of this aspect with the amount of rainfall led to the rapid rise in the hydrometric levels of the Burano River course and its tributaries. Sudden and destructive floods were triggered, leading to numerous landslide phenomena that contributed significantly to the downstream solid transport, although widespread residual risk conditions persisted along the slopes (Donnini et al. 2023).

The town of Cantiano was one of the areas affected the most by floods. In a very short time, the local riverbeds were crossed by large, turbulent flows and filled up by transported solid load, quickly exceeding the containment limit and overflowing uncontrollably. Many buildings in the historic centre were flooded by water, mud and debris and the urban paths of the watercourses were severely damaged, sometimes in association with connected sewers (Fig. 4). At the same

Fig. 4 Location of the effects of the high flow rates in the artificial stretch of riverbeds and sewer system within the built-up area of Cantiano. (a) pavement and road torn off by the overflowing water of the Bevano creek; (b) outlet of the underground riverbed of the Tenetra stream and related material transported; (c) break in the sewerage network in front of the Municipality; (d) natural protections set up during the emergency; (e) breaking point of the culvert caused by the high hydraulic pressure created.

time, the city became isolated due to landslides along the external main communication routes and bridge damage due to flooding activity and mass movements, even in combined action.

Several circumstances were primarily decisive in generating the critical issues of this site: i) the stationing of exceptional precipitation in the surrounding mountains over an arid terrain, ii) the local geology in its capacity to create debris, iii) the proximity, with its historic centre, to the confluence of two creeks (Bevano and Tenetra) with the main river (Burano) (Fig. 4), iv) the geomorphologic conformation of the reference water catchment areas and their natural hydraulic network (deeply discussed in section 4.1), and v) the response of hydraulic layout of urbanised stretches where the three watercourses converge (Fig. 4). The latter is a consequence of a historic anthropic activity intervening heavily on the original fluvial path and geometry that almost definitively cancelled out any character of naturalness and functional specificity over time (Morelli et al. 2023).

The Burano River was diverted in the upstream stretch of the town in the late 1920s through an 80 m tunnel (about 8 m wide and 9 m high) (Morelli et al. 2023) at a high angle to the original path (Fig. 5). The original course, consisting of a meander that ran alongside the town's ancient buildings on one side and the rocky slopes of a mountain relief on the other, was permanently blocked by a high wall and filled with material behind it. The upstream portion preceding the underground diversion work is confined between artificial masonry banks. In the late 1700s, the Bevano Creek, which originally passed through the middle of the current Luceoli Square in the city's centre, was diverted about 50 m North into a confined (Morelli et al. 2023), narrow, recessed curving path. The shape has remained unchanged until today. At the end of the 1950s, it was covered with concrete slabs for a length of 200 m, as the concept of hygienic safety was increasingly pressing. At that time, there was no complete sewerage network or purification system. Subsequently, some houses were also built on some parts of the covered areas. In the mid-1700s, the Palazzo del Conte was built above the Tenetra Creek, creating the first underground riverbed in this area. This closure, built in masonry with an arched vault, was then modified over time until its current size (which was about 57 m in length) and the urban downstream section was channelised up to the confluence with the Tenetra Creek, beyond which it was confined until reaching the Burano River in more recent times.

3 Methodology

A comprehensive methodology that integrates

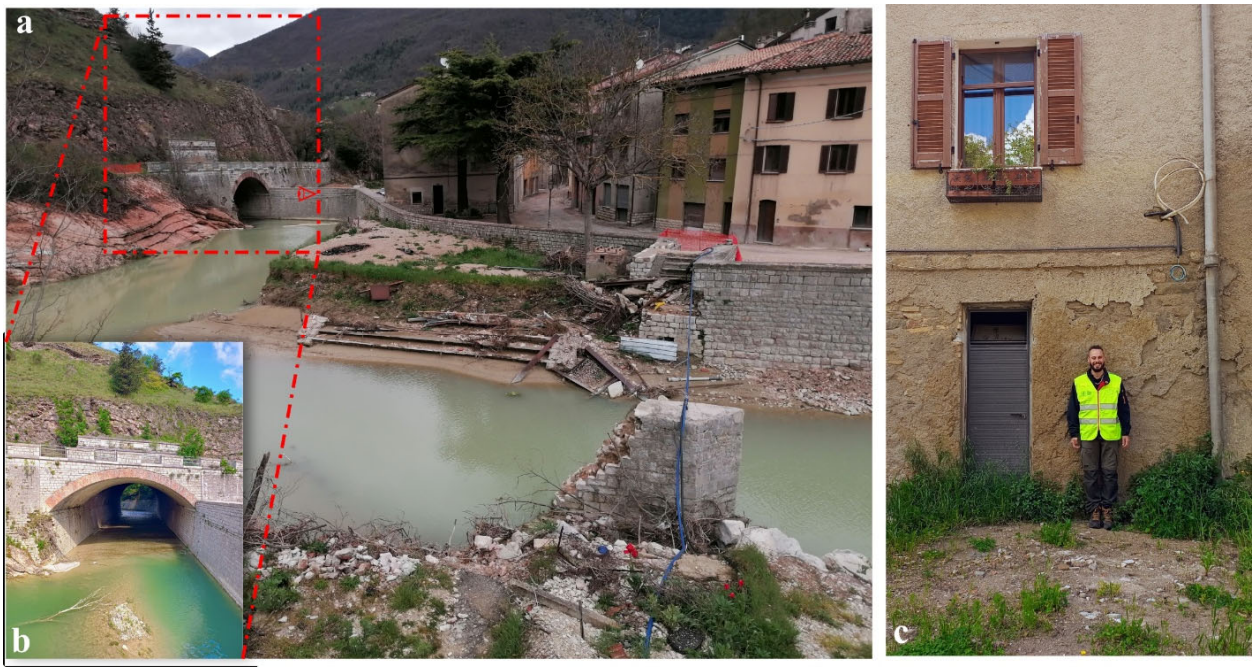

Fig. 5 (a) River stretch before the detour, flood damage can be seen; below is a destroyed bridge; (b) Burano detour tunnel as seen from the road; (c) hydrometric level reached homes near the detour area.

multiple spatial analyses is introduced to investigate the interactions between slope dynamics and the river network at the watershed scale, while also evaluating the transport capacity of sediments that can be mobilized within the system. The procedure consists of two main stages. The first is aimed at providing a detailed geomorphological characterisation of the area, considering both pre-event and post-event instabilities. The second comprises a GIS-based analysis aimed at understanding the spatial distribution of instability processes and the controlling patterns they exhibit in relation to the main watercourse.

Finally, a sediment availability map is obtained, where "sediment availability" means accessibility of sediment present in source areas or along a catchment area that can be detached, mobilized, and then transported during hydrological or geomorphological events. The material has the potential to enter the transport chain when conditions (e.g. rain, runoff, erosion) allow. Fig. 6 shows the flow chart relating to the structured work model.

3.1 Geomorphological characterisation – morphological aspects

A detailed geomorphological map was arranged, basically including i) geomorphological complexes, corresponding to geological formations from the official Regional Geological Cartography (scale 1:10,000), grouped according to their degree of erodibility based on regionally different states of weathering, and adjusted based on observed hillslope conditions following the method of Moosdorf et al. (2018). In this approach, erodibility values are calibrated using real slope data for each lithology class to better represent the sediment production potential at the landscape scale. ii) Quaternary deposits extracted from the same source, and iii) existing and updated landslide distribution. The datasets corresponding to points i) and ii) represent a reasoned reprocessing of pre-existing information, whereas the dataset in point iii) is based on published inventories and has been verified through field inspections conducted as part of this study. A quantitative descriptive statistical analysis of the landslide inventory triggered by the 2022 extreme rainfall event (E-LIM database) was carried out to identify well-constrained sediment-mobilization areas, focusing specifically on the fraction of material with the highest mobility and runout capacity. Morphological features at all spatial scales were represented on the map as polygons when larger than 225 m^2, and as points when smaller.

QGIS software (version 3.34.6) was used for this product following the guidelines indicated by the Italian Institute for Environmental Protection and Research of the Ministry of the Environment (Campobasso et al. 2021). A 10 m-resolution DTM (prior to 2022), called TINITALY DEM and released for free in the updated version in 2023 by the National Institute of Geophysics and Volcanology, was used as a basic spatial datum (Tarquini et al. 2007, 2023; Tarquini and Nannipieri 2017). Multiple landslide datasets were incorporated, available by catalogues

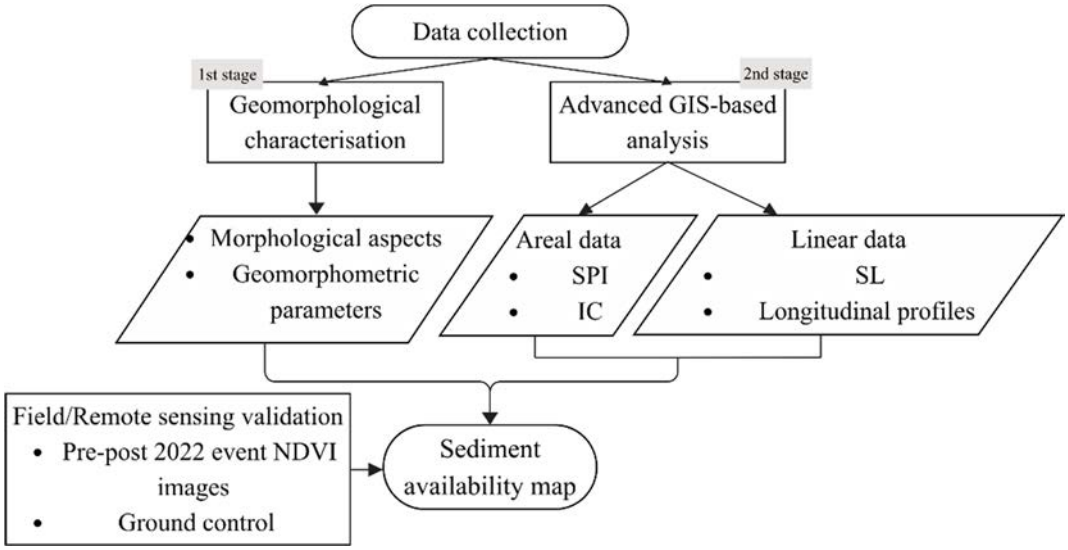

Fig. 6 Methodological flowchart highlighting all the steps of the applied procedure that lead to the sediment availability assessment, validated by field checks and remote sensing analysis.

with different information: the Italian Landslide Inventory with the characterisation type and other descriptive aspects (The IFFI Project, scale 1:25,000; Trigila et al. 2007, 2010; Trigila and Iadanza 2008) and the 2022 post-event inventory (E-LIM Inventory, scale 1:15,000; Santangelo et al. 2023).

3.2 Geomorphological characterisation – geomorphometric parameters

From the river network and catchment layers, the main geomorphometric parameters (Table 2) were calculated in a GIS environment. Relief ratio (Rh), bifurcation ratio (Rb), stream frequency (Fs) and drainage density (Dd) were used to parameterise the dimensional, morphological and topological properties of the drainage network and catchment areas. Rh expresses the overall relief energy of the basin and provides an indication of the potential for sediment mobilisation along slopes. RB describes the degree of branching of the drainage network, reflecting the efficiency with which runoff and sediment are channelled downslope. Fs represents the density of channels per unit area and therefore indicates the degree of hillslope dissection and the proximity of sediment sources to the fluvial network. Finally, Dd quantifies the total channel length per unit area and serves as a proxy for the capacity of the drainage system to intercept and convey sediments. Taken together, these morphometric indices provide quantitative measures of basin physiography and offer insight into the structural components that control sediment connectivity, thereby characterising the predisposition of the catchments to transfer sediments from hillslopes to the main channel.

This analysis was used to preliminarily define the spatial and typological availability of sediments. By overlaying these layers within a GIS environment, the intersection of the different parameters highlights locations where predisposing factors co-occur, delineating hotspots that are most prone to sediment availability and potential mobilisation. These critical areas are typically associated with zones of flow acceleration, hydraulic jumps, and topographic convergence, where water and sediment are preferentially concentrated. The areal GIS analysis made use of this information as a basis for controlling the results.

3.3 Advanced GIS-based analysis – areal assessment

The first phase of GIS analysis characterised the entire catchment area (areal approach), understanding the physical connections of potentially mobilizable sediment inside it to the primary channel network and the link between the power of flowing water and the soil erodibility deduced with the Moosdorf et al. (2018) method. For such spatial analyses, the above-mentioned TINITALY DEM was used as a basic spatial datum.

In particular, the areal basin analysis envisaged the assessment of two morphometric indices:

- Stream Power Index (SPI), based on modified

Table 2 Methods and equations for the calculation of geomorphometric parameters (Shekar and Mathew 2024).

Basin's morphometric parameters	Formula/description
H (m. a.m.s.l.)	Basin maximum elevation
h (m. a.m.s.l.)	Basin minimum elevation
Lb (m)	Basin length
A (km^2)	Basin area
P (km)	Basin perimeter
Relief Bh	Bh = $H - h$
Relief ratio Rh (Schumm 1956)	Rh = Bh / Lb
Circularity ratio Rc (Miller 1953)	Rc = $4\pi A / P^2$
Elongation ratio Re (Schumm 1956)	Re = 2 [A / π]$^{0.5}$/ Lb
Gradient ratio Gr (Sreedevi et al. 2005)	Gr = (a-b) / Ls
Basin major stream's morphometric parameters	**Formula / description**
a (m. a.m.s.l.)	Major stream's source elevation
b (m. a.m.s.l.)	Major stream's mouth elevation
Ls (m)	Major stream's length
Total Stream number Nu (Horton 1945)	∑Nu$_n$ (Nu$_n$ stream number of the n order)
Total Stream length Lu (km)	∑Lu$_n$ (Lu$_n$ stream length of the n order)
Bifurcation ratio Rb (Horton 1945; Strahler 1964)	Rb = Nu / N(u + 1)
Stream frequency Fs (Horton 1945)	Fs = ∑ Nu / A (A area of the basin)
Drainage density Dd (Horton 1932)	Dd = Lu / A

Abu El-Magd's equation (Abu El-Magd et. al. 2021), using ArcGIS Pro version 3.3 to compute it.

- Index of Connectivity (IC), based on Borselli's original equation (Borselli et al. 2008) modified by Cavalli et al. (2013) in the SedInConnect software version 2.3 (free, open-source and GIS-independent stand-alone tool) (Crema and Cavalli 2018).

(1) Stream Power Index (SPI)

SPI is one of the most popular attributes that can be calculated with single- and multiple-flow direction algorithms, and it assumes that discharge is proportional to the specific catchment area (Wilson 2012). SPI is conceptualised to visualise potential flow erosion and its relationship to landscape processes in the entire basin. The SPI regulates the potential erosive force of water flow and describes the potential for flow erosion at the specified surface point (Moore et al. 1991) to determine how regions with topographic potential for erosion and deposition are spatially distributed in a complex terrain.

The SPI concept (Moore et al. 1991) is expressed in the following formula:

$$\mathrm{SPI} = \mathrm{SCA} \times \tan\beta \quad (1)$$

where SCA is the specific catchment area, while β is the slope expressed in radians.

The SPI is obtainable from GIS using the tool "Raster calculator". The hydrological modelling tools integrated into ArcGIS Pro derive flow direction, flow accumulation, and slope functions from the DTM. Eq. (2) results from applying the variant (Abu El-Magd et al. 2021; Chowdhury 2023). 0.001 is a constant introduced into the logarithmic function to reduce extreme values and handle values close to zero. In this case, the slope is in degrees, and division by 100 facilitates multiplication using the logarithm. The logarithmic function is applied to the first factor so that their distribution would more consistently reflect the trend; the slope contribution is kept in linear form (after a simple normalisation) to represent its impact on the SPI adequately.

$$\mathrm{SPI} = Ln\,(As + 0.001) \times (\beta/100 + 0.001) \quad (2)$$

where As is the basin flow accumulation, β is the basin slope, and "Ln" is a constant that refers to the Napierian logarithm. The flow accumulation demonstrates regions that contribute to the overland flow (Abu El-Magd et al. 2021). This formula represents a valid empirical simplification that proves to be more compliant for workflows in a GIS environment. The SPI determines the erosive power of the channel and expresses the topographic potential for deposition (for low or negative values) and erosive areas (positive values).

(2) Index of Connectivity (IC)

The sediment-transport IC quantifies the propensity of sediment to be transferred from one part of the landscape to another, typically integrating factors such as slope, land use, and the structure of the drainage network. In particular, the IC index is used to calculate the structural morphometric connectivity of sediments. For each raster cell, the degree of connection that controls sediment flows across the landscape is calculated by the SedInConnect software (Crema and Cavalli 2018). The IC shows the potential connection between sediments eroded from hillsides in relation to a selected target feature, which is the main hydrographic network in this case study. Within the same watershed, each point (pixel of the basin) yields a probability value ranging from negative to positive infinity, while the target feature defined in the model determines the connectivity configuration (Cavalli et al. 2013). When a vector layer (in shapefile format for SedInConnect) defining the topographic depressions to be emphasised is supplied, the model first identifies the portions of the DTM that effectively drain sediment toward these features. All areas that do not contribute flow to the selected depressions are then discarded and excluded from the IC computation (Crema and Cavalli, 2018). In this work, the target was used in order to focus the analysis on the lateral slope to the main network, thus making it possible to distinguish smaller connective channels. This was represented by a linear shapefile with a buffer of 20 m on the main river, 10 m on its tributaries, and 5 m on less developed high-altitude watercourses. Therefore, maximum attention was given to the slopes by observing where high connectivity values were detected. River flow and sediment may be connected as indicated by the IC proposed by Cavalli et al. (2013) (Eq. 3). The index operates at the catchment scale by representing the transfer of material from slope-derived source areas to the main channel, which corresponds to the topographic minimum in the model. The equation includes two main components: the upslope (Dup) and downslope (Ddn) terms. Dup quantifies the upslope component of connectivity, describing the potential for sediment mobilisation and routing from the contributing area. It integrates both slope and flow-path length, rather than representing a simple distance measure. Ddn represents the resistance to sediment

transfer, expressed as the effective distance that a particle must travel downslope in order to reach the drainage network. Because IC is defined within the range [−∞, +∞], larger IC values indicate higher connectivity (Cavalli et al. 2013). Consequently, the probability that sediment will reach the main river course increases as the downslope distance decreases.

$$IC = \left(\frac{Dup}{Ddn}\right) \quad (3)$$

SedInConnect (Crema and Cavalli 2018) computes the Index of Connectivity (IC) as defined by Borselli et al. (2008) and modified by Cavalli et al. (2013), using DTM-derived topographic components. The software implements a flexible weighting factor (W) to model the impedance to sediment fluxes. By default, W is represented by a surface-roughness proxy, reflecting topographic variability, although alternative configurations (e.g., a land-cover–derived C-factor) can be applied depending on data availability and study aims. In this work, W is interpreted as the flow-impedance factor associated with surface roughness and was computed internally by SedInConnect from the DTM (Crema and Cavalli 2018). Roughness was estimated as the standard deviation of elevation within a moving window, thereby capturing local variability in slope and micro-topography. Accordingly, the parameters required for the processing included the DTM, the roughness layer, and a selected target represented by the river network derived from hydrological extraction of the DTM. The choice of this parameterization is motivated by the morphological setting and the limited anthropogenic influence in the study area, which makes land-use–based factors less descriptive. Indeed, the existing land-use classification (CORINE Land Cover inventory; ISPRA 2019) is essentially homogeneous within the study area and does not introduce appreciable spatial contrasts for the purposes of this research; therefore, it was not considered in the analysis. The underlying morphometric routines in SedInConnect are conceptually compatible with TAUDEM-style terrain analysis for flow direction and contributing-area derivation.

3.4 GIS-based advanced analysis – linear assessment

The second phase of the GIS analysis focused on the main river courses, using data derived exclusively from the river network extracted from the TINITALY DTM (linear approach). A longitudinal analysis was carried out, and the Stream Length-Gradient (SL) Index (Piacentini et al. 2020) was adopted as the main morphometric parameter, calculated according to the formulation proposed by Hack (1973). The results were subsequently compared with geometric information obtained from the observation of longitudinal river profiles derived from the digital model, using the qProf plugin of QGIS which was used to generate topographic profiles. While the SL index evaluates the average behaviour of predefined river segments, the analysis of longitudinal profiles allows the identification of minor irregularities in the profile, such as abrupt hydraulic jumps (spatially narrower observations).

(3) Stream Length-Gradient (SL) Index

The linear analysis was carried out by generating longitudinal profiles used to calculate the SL index (Troiani et al. 2014). This index analyses the most significant topographic variations along the river course as the morphological signature of surface and subsurface processes. The SL index is strongly related to the hydraulic gradient and often indicates perturbations along the river channel. SL represents a proxy for stream power per unit length and is proportional to the total stream power available within a specific reach (Summerfield 1991; Pérez-Peña et al. 2009). The index was implemented in a GIS environment using an ArcGIS tool. The DTM represents the only input dataset, and the output unit is expressed in metres. In the practical procedure, points spaced at fixed intervals were place along the river network. The elevation value was interpolated for each point, and the equation reported below was applied. According to previous studies (Troiani et al. 2014) conducted in comparable settings characterised by small catchments and torrential streams typical of predominantly mountainous environments, such as the study area, the ΔL value in Eq. 4 that providing most accurate results correspond to a distance of 50 m. This distance improves the efficiency of the tool. However, the optimal value strongly depends on the size of the study area and on the resolution of the topographic model. The use of this parameter reduced the number of errors in the analysis. Eq. 4 (Piacentini et al. 2020) was applied to identify significant deviations from the typical concave-up shape of longitudinal profiles of bedrock rivers within mountainous catchments. These deviations correspond to differential anomalies distributed along

the entire drainage network. On the map, these anomalies are referred to as knickzones and knickpoints. These features can generally be attributed to a several factors, the most significant being: i) lithological contrasts in the substrate (geology), ii) the presence of a tectonic structure (tectonics), and iii) the existence of a landslide in the riverbed (morphological evolution).

$$SL = \Delta H \times L / \Delta L \quad (4)$$

where ΔH is the variation of elevation between two points along the stream channel, ΔL is the distance between the two points, and L is the total channel length from the channel initiation point (Piacentini et al. 2020).

The first output of the SL model consists of a set of point values. Following the classification proposed by Piacentini et al. (2020), a quartile distribution was adopted to subdivide the results into classes representing different potential erosional dynamics. A graduated symbology withfive classes was therefore used to highlight the highest values. This method divides the attributes into classes containing the same number of features. The points with the highest steepness anomaly values, included in the fifth class (V class), are represented by a light purple colour.

3.5 Validation method

The validation of the obtained results was carried out using two approaches. The first included a remote verification analysis using optical multispectral satellite images aimed at characterising the situation before the event. The Normalised Difference Vegetation Index (NDVI) was used, calculated by optical multispectral Planet images (Planet Team 2022). This index represents a graphical indicator for the analysis of the green vegetation conditions. PlanetScope provides up to 3 m multispectral imaging with daily revisits and is made up of many CubeSat (Doves and Super Doves) flights in sun-synchronous orbit. The earlier-generation Dove satellites (Standard PlanetScope) gather multispectral imagery in four bands: blue, green, red, and near-infrared. Launched since 2020, SuperDoves (upgraded PlanetScope satellites) provide 8-band multispectral imaging with calibrated and smaller bands in the wavelength range of 430–860 nm. By carefully selecting two days, one before and one after the event, with 0 cloud cover, it was possible to assess the changes in terms of vegetation variations in just a few days. Planet images are supplied already orthorectified and radiometrically calibrated with corrected reflectance. The bands used were red and NIR (Confuorto et al. 2025). A formula that measures the difference between near-infrared (NIR) and red light reflectance is used to generate the NDVI, which quantifies vegetation. NDVI is calculated as follows: (NIR - Red) / (NIR + Red). Similar to other satellite data, Planet imagery can be used to compute NDVI, which offers information on the density and health of the vegetation. NDVI change detection was performed to localise landslides that occurred, where the vegetation on the slope is removed or partially destroyed, leading to a decrease in the NDVI value (Confuorto et al. 2025). The software chosen for use is ENVI (Environment for Visualising Images).

The second methodology adopted a conventional framework. Utilizing a heuristic approach, the most critical areas were identified through terrestrial and UAV photogrammetry. Subsequently, pre-defined control points, deduced from the final map, were compared against these findings for validation. A fundamental component of this study also involved benchmarking the predictive results against the spatial distribution of landslides triggered during the 2022 extreme weather event, as documented in the E-LIM Inventory.

4 Results

4.1 Geomorphological characterisation – morphological aspects

Based on the classification criteria defined by ISPRA (Campobasso et al. 2021), four lithological complexes were identified within the study area: pelitic-arenaceous, marly-mudstone, limestone-anhydrite, and arenaceous rocks. Each unit corresponds to a distinct geomorphological complex, represented by a specific background colour on the drawn geomorphological map (Fig. 7). This representation constitutes the basis on which the various specific thematic levels were subsequently superimposed. Regarding the post-event landslides, the E-LIM inventory provided the exact mapping of 351 landslides physically reachable during a field survey or visible from observation points on the ground. Of the total number of landslides digitised after the event 156 polygons and 195 points are located, and 50% of them are attributable to the earth slide type, 15% to the debris flow type, 10% to the debris slide type,

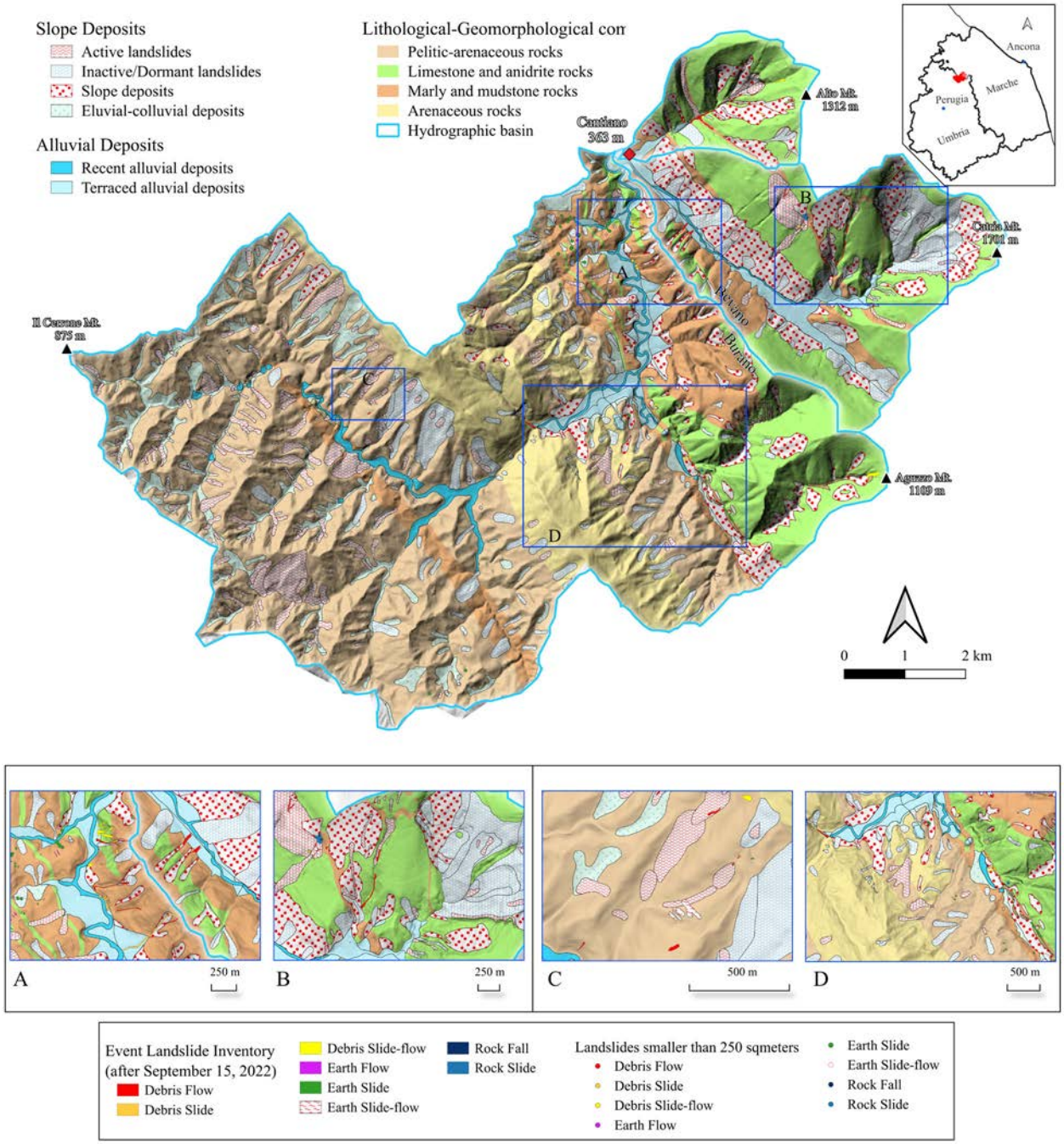

Fig. 7 Geomorphological map to understand sediment production (top), images from A to D (bottom), zoom on different sectors of the basin (see the left map for the position) where the small landslides inventoried by E-LIM are visible in detail.

11% to the earth slide-flow type, 7% to the debris slide-flow type, 6% to earth flow type, and 1% to the rockfall and rockslide types according to Hungr et al. (2014) classification. The events with the highest number of occurrences (earth flow/slide) are in the western part of the catchment area due to the local lithology. On the contrary, around Cantiano, debris flows, debris slides and rockfalls are more frequent due to the main limestone composition.

Across the three investigated catchments, landslide areas affect 5.3% of the Burano River basin, and approximately 4.4% and 4.5% of the Bevano and Tenetra river basins, respectively. Considering their real extent, sediment availability appears to be greater

in the Bevano and Tenetra basins. In the Bevano river basin, zones of material deposition were identified both at the foot of Mount Catria, approximately 4 km upstream of Cantiano and along the valley-bottom road, due to the activation of run-off deposits (Fig. 7). In contrast, the upper portion of the Bevano creek shows no major morphological changes, as it hosts an extensive landslide area that, according to available data, has exhibited no significant evolution for at least the past two decades. In the Tenetra Creek basin, the situation differs owing to the steep slopes in the upper reaches and the abundance of available unconsolidated sedimentary material. Sediment transfer is more pronounced and concentrated along the main drainage network, while it is less evident on the slopes, except for the main channel incised into the highly erodible marnous unit of the "Marne a Fucoidi" formation.

4.2 Geomorphological characterisation - geomorphometric parameters

Geomorphometric parameters for characterising the basins' geomorphology and comparing the dynamic characteristics of their drainage patterns are listed in Tables 3 and 4 (Shekar and Mathew 2022). The parameters defining the drainage texture (*Nu*, *Lu*, and *Fs* parameters in Table 4) denote numerous shorter streams for the Burano basin compared with the stream patterns of the Bevano and Tenetra basins. This could be related to the less permeable bedrock of the basin, which is characterised by a significant surface runoff compared to the other basins. The drainage density (*Dd*) values of the Bevano and Tenetra basins (Table 4) can be mainly related to relief ratio (*Rh*) values higher than those of the Burano basin (Table 3). The latter parameter quantifies the topographic evidence that the Bevano and Tenetra basins are shorter with higher gradients than the Burano basin. Lastly, the lower circularity (*Rc*) and elongation (*Re*) ratios' values of the Burano and Bevano basins (Table 3) indicate a lower propensity for runoff, erosion and sediment transport; on the contrary, the more 'oval-circular' shape of the Tenetra basin implies a greater concentration of flows and therefore a greater likelihood of runoff with energetic flows and thus may imply sediment transport. The much lower value of the slope ratio (*Gr*) of the Burano River confirms its lower sensitivity to runoff and a higher probability of flooding of flat areas due to a decrease in the system's energies, which in turn leads to a deposition of material.

Table 3 Basin's morphometric parameters calculated to characterise and compare the hydrological behaviour of the three basins. Abbreviations and definitions of the morphometric parameters are provided following Shekar and Mathew (2024).

Basin's morphometric parameters	Burano	Bevano	Tenetra
H (m.a.m.s.l.)	1,101.36	1,701.53	1,319.90
h (m.a.m.s.l.)	360.15	360.16	360.37
Lb (m)	30,964.67	7,679.06	3,521.53
A (km²)	102.93	20.69	6.25
P (km)	43.80	19.74	9.35
Relief Bh	741.21	1,341.37	959.53
Relief ratio Rh (Schumm 1956)	0.02	0.17	0.27
Circularity ratio Rc (Miller 1953)	0.67	0.67	0.90
Elongation ratio Re (Schumm 1956)	0.37	0.67	0.80
Gradient ratio Gr (Sreedevi et al. 2005)	0.03	0.11	0.25

Table 4 Stream's morphometric parameters calculated to characterise and compare the drainage patterns of the three basins. Abbreviations and definitions of the morphometric parameters are provided following Shekar and Mathew (2024)

Basin major stream's morphometric parameters	Burano R.	Bevano C.	Tenetra C.
a (m. a.m.s.l.)	874.00	1,225.00	1,225.00
b (m. a.m.s.l.)	350.00	360.00	350.00
Ls (m)	20,467.00	7,679.10	3,521.50
Total Stream number Nu (Horton 1945)	5,153.00	876.00	220.00
Total Stream length Lu (km)	507.46	126.82	30.75
Bifurcation ratio Rb (Horton 1945; Strahler 1964)	1.95	1.89	1.67
Stream frequency Fs (Horton 1945)	50.03	41.71	36.67
Drainage density Dd (Horton 1932)	4.93	6.04	5.12

4.3 Stream Power Index map

The Stream Power Index (SPI) map (Fig. 8) highlights areas where surface runoff is likely to concentrate and exert enhanced erosive power. High SPI values identify slope sectors and channel reaches where flow energy and velocity increase, thereby enhancing the capacity for sediment entrainment and transfer from both hillslope deposits and channel sediments across the drainage basin. These areas are mainly concentrated in the impluvia, where the slope and convergence increase. The SPI of the Burano basin ranges from −4,59448 to +4,99374. A pixel statistical

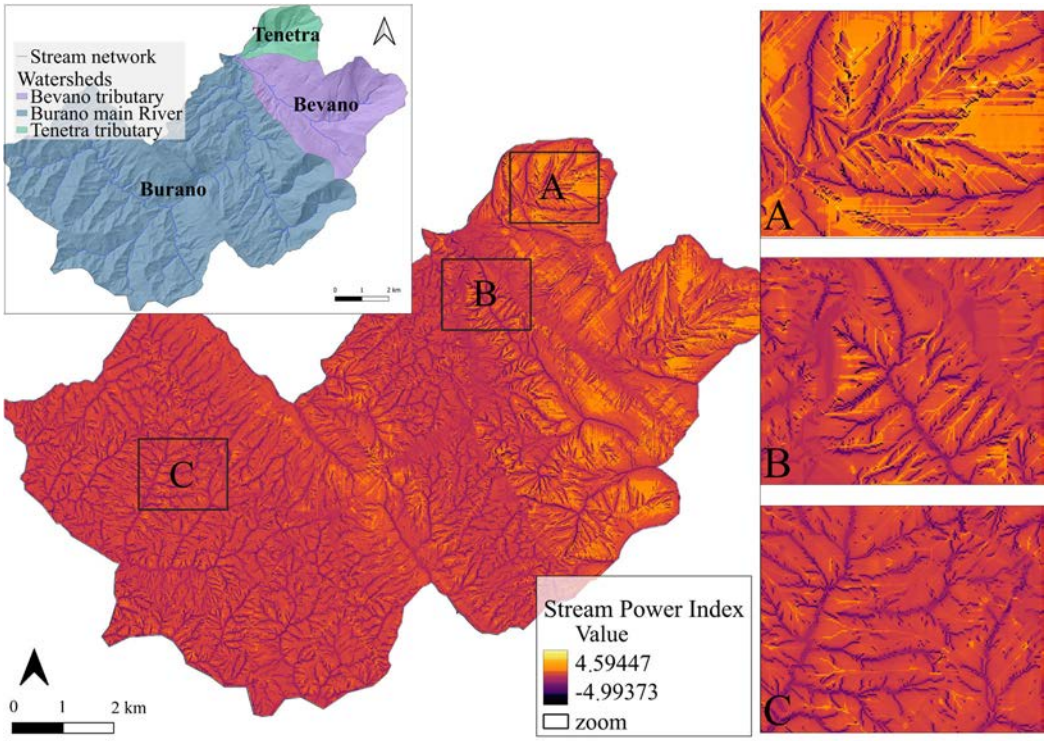

Fig. 8 Stream Power Index Map. Reflects the erosive power of streams defined for the upper Burano basin.

analysis was used to establish a quantification of the spatial range. A calculation was conducted based on the three catchment basins, excluding values less than +1 from the raster to isolate the most vulnerable places. The upper Burano basin comprises 4.3% of these raster map cells, while the Bevano and Tenetra basins account for 17% and 22.5%, respectively. This distribution can be explained by both the overall steepness of the area and its lithological characteristics, as discussed in detail in the preceding sections. In the three catchments, zones that accelerate the water flow cover 4.1 km² in Tenetra, 14.8 km² in Bevano, and 59.8 km² in Burano basins.

4.4 Index of connectivity map

The output map (Fig. 9) was classified according to positive and negative logarithmic values ranging from 2.48 (high) to −5.43 (low). Positive values indicate that sediment is well connected, whereas negative values reflect areas that are effectively not connected to the downslope transport network.

Based on the spatial distribution of the output values, the Tenetra basin, the upper part of the Bevano basin, and the higher-order impluvia along the Burano River exhibit high connectivity indices, indicating effective connections between sediment source areas and transport pathways that facilitate sediment movement. In contrast, sediment transfer is progressively hindered in areas characterised by low positive connectivity values, which reflect weak structural connections. Areas exhibiting negative values represent decoupled conditions; in this context, the term disconnected implies the presence of an interruption within the transfer pathway, whereas unconnected refers to the complete absence of connectivity.

It should be noted that the Index of Connectivity analysis is performed using a predefined target. In this study, the target corresponds to the river network, which was extracted by applying a threshold value that defines the level of network detail and allows the identification of potential zones of material accumulation along the slopes. As a consequence, positive connectivity values are concentrated around the extracted stream orders and generally do not extend to the highest portions of the watershed. Different degrees of connectivity and spatial detail can be recognised on the map through the graduated colour scale. In the Burano basin, the mobilised material locally reaches roads and settlements and can be traced back to active superficial landslides. From this raster map, 2.5% of the total cells of the Burano basin area, 2% of the Bevano, and 2.7% of the Tenetra

exhibit high sediment connectivity. In terms of spatial extent, 0.12 km² in Tenetra, 0.3 km² in Bevano, and 1.67 km² in Burano were affected.

4.5 Stream Length-Gradient (SL) Index map

The output map (Fig. 10) was represented by points along the river paths with values associated with different colours, thus immediately highlighting the areas where the main jumps are present. These do not include points that correspond to hydraulic works on the 1:10,000 scale topographic map, nor those considered invalid through a geomorphological interpretation (manual filtering). The obtained values

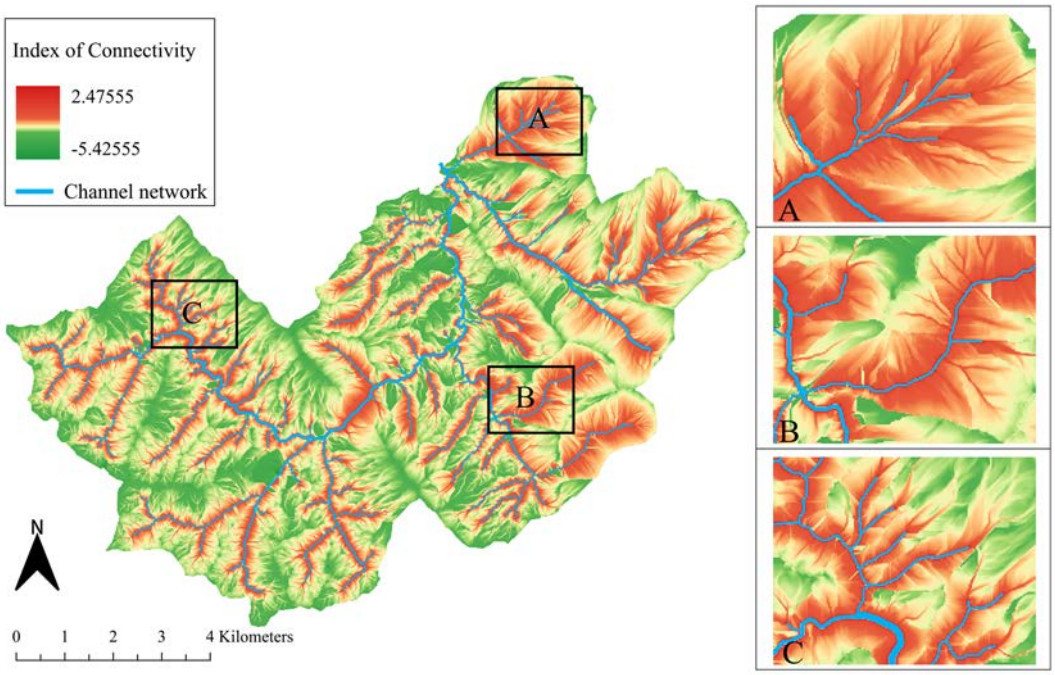

Fig. 9 Index of Connectivity. Unconnected areas are highlighted in green, while connected areas are highlighted in red.

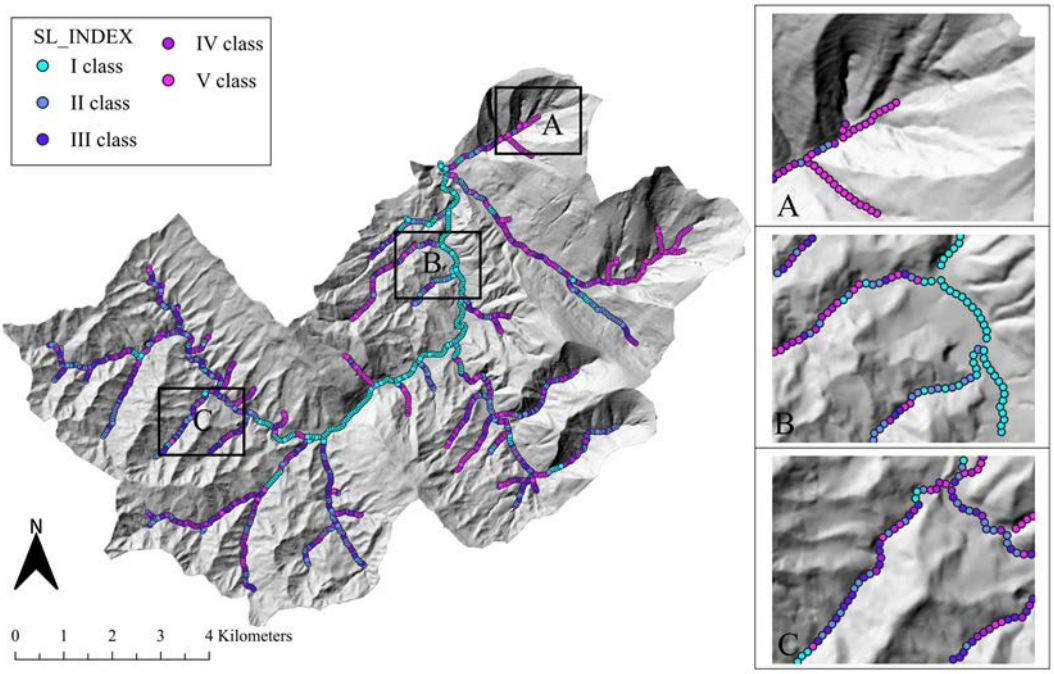

Fig. 10 Stream Length-Gradient Index map processed using the SLiX tool (Piacentini et al. 2020) and setting a five-class quantile classification. Greater values represent areas with the presence of knickpoints.

were positive from a minimum of 0 (I class), areas where the gradient is shown to be low, to a maximum of 1,278 (V class). Most knickpoints with high values are found in the major river orders. The knickzones that acquire greater importance are where along-stream deviations are extensive from the typical concave-up shape in isolated river reaches (knickzones). In these cluster areas, an accumulation of material coming from secondary connection channels or lateral landslides could be considered responsible for the appearance of sudden high gradients. This difference in heights could indicate a (more or less recent) unconsolidated deposit which represents a potential source area of material. River reaches with the fifth class are found in all the trunk streams of the three studied sub-basins, indicating that the potential for sediment entrainment is evenly distributed throughout the area (although in the Burano it is more concentrated in the central section). However, these values have a different overall relevance when associated with the hillslope assessments.

The percentages of anomalies along the network were highlighted by the five classes quantile classification. According to this, Burano accounts for 56.5% of the anomalies, Bevano for 33.4%, and Tenetra for 10%. Observing anomalies with values greater than 400, the highest percentage was identified in Bevano (17.8%), while Burano and Tenetra were characterised by 10% and 7.5%, respectively.

4.6 River longitudinal profile

The longitudinal profile visualisation emphasised the spatial variation of morphology along the main river courses (Burano, Bevano, Tenetra), highlighting significant deviations in the topographic profile trend (Fig. 11). It is a way to visualise the abrupt slope transition of the riverbed, as local discontinuity in the general evolutionary context (therefore clearly detectable even for riverbed segments smaller than 50 m used for the SL index). Tenetra and Bevano have higher elevation springs and much shorter paths, making hydro-geomorphological processes more aggressive. In particular, the analysis of longitudinal profiles has proven helpful in identifying areas with localised hydraulic jumps, some of which are characterised by hydraulic structures, while others are of natural origin without any anthropogenic influence on the site or nearby.

4.7 Sediment availability map

A synoptic map that clearly integrates all the primary processed data was created to support the interpretation of the zones that generate sediment and how these sediments can (or cannot) move. In particular, by classifying the resulting Index of Connectivity and Stream Power Index maps and emphasizing the most sensitive ranges, a functional zoning of the river basin—comprising source, transfer, and storage areas—was derived, providing an integrated representation of sediment dynamics and the morphodynamic energy of the flows. Fig. 12 illustrates the sediment availability map, categorised to highlight the peak distribution values for enhanced analytical clarity. In this framework, SL Class V is isolated and further partitioned into five discrete sub-classes based on a quantile distribution. The factors governing the combination of the two indices are closely related to the raster DTM derivatives, slope and flow accumulation. For a more accurate interpretation of the most productive and river-connected areas in terms of sediments, it was therefore conceivable to place the indices' maps in a topological relationship with one another. In addition to the two parameters mentioned above, another important source of information is the mass movements extracted from the landslide inventories (official Italian IFFI catalogue) of the area. Quiescent landslides and alluvial deposits were excluded from the analysis, taking into account only landslides with signs of evolution. The accumulations recorded in this area due to the topography are strongly related to the lithology of the area. The last defined index is the SL, which is an indicator of anomalous gradients in the networks of the channels analysed that can indicate a possible inflow/accumulation of material into the main riverbeds. The use of the more classical longitudinal river profiles supported the interpretation of the detected morphological variation, identifying local and punctual morphological anomalies that can be associated with lithological jumps (especially those represented by rocks emerging from the riverbed) or anthropogenic works, which on the contrary can indicate the presence of strong current, erosion and taking charge of the materials downstream of the jump. In this sense, the integration of the two longitudinal analyses works very well in the interpretation of the variations. Regarding map reading in the connectivity index, values were isolated from -1 to the maximum positive value to highlight the major and minor

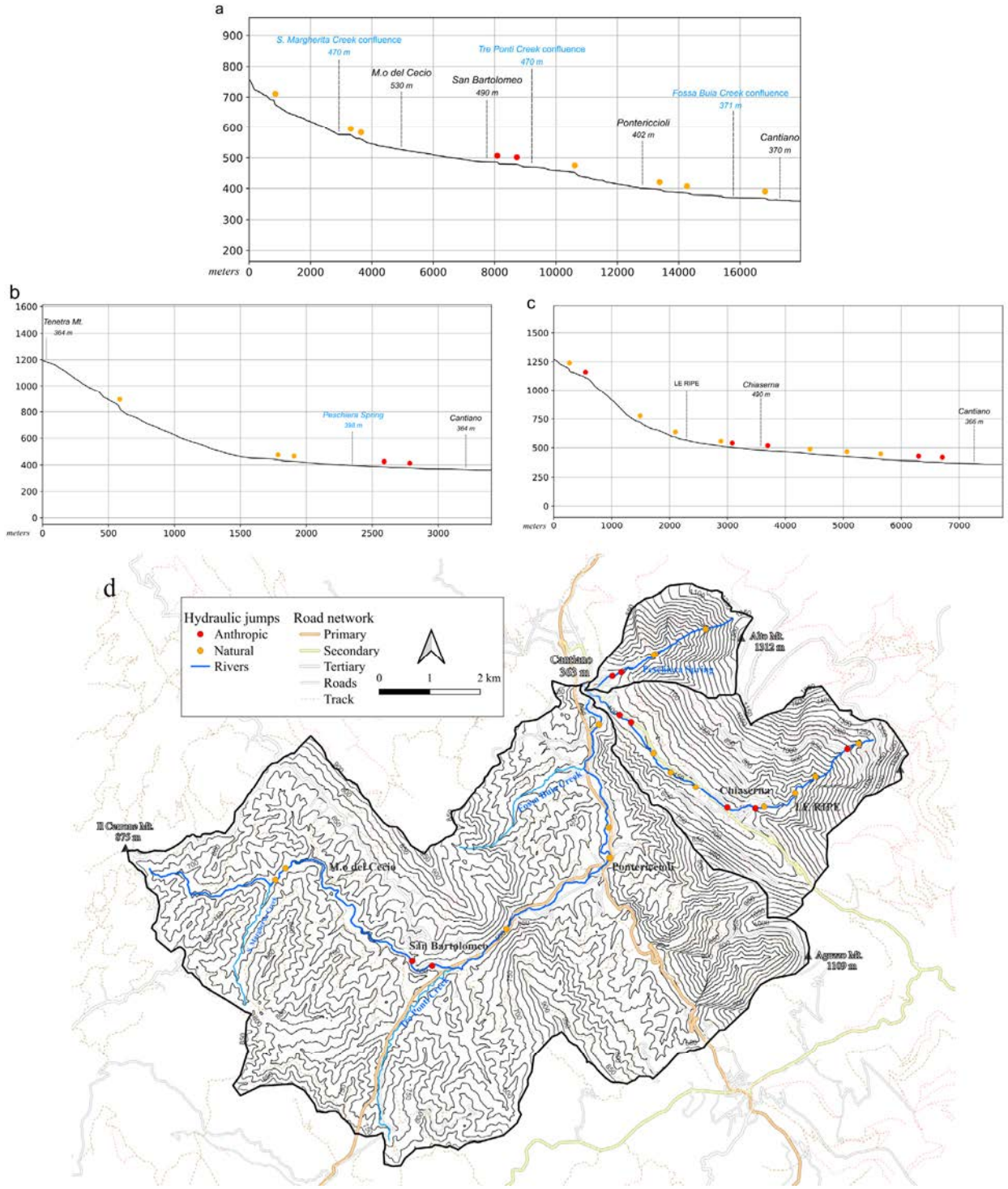

Fig. 11 River longitudinal profiles: (a) Burano River; (b) Tenetra Creek; (c) Bevano creek; (d) Location map. Red and orange dots mark anthropic and natural hydraulic jumps, respectively. The toponymy derives from the official cartography of the Italian Military Geographic Institute (IGMI): in black, towns, built-up areas, and mountains; in blue, confluences with other water bodies.

channels of connection on the slopes. The power index, on the other hand, showed a different distribution of values, concentrating on the area of positive values; those greater than 1 were isolated. Similarly, the stream length-gradient index was classified in a graduated manner, and all classes except the one with the highest values were excluded, which isolated the most important knickpoints (Fig. 12).

Analysing the whole studied hydrographic system, the Burano River flows through younger materials with marly arenaceous compositions, which allows it to more easily modify its course and riverbed, promoting significant fluvial dynamics. The Burano River flows through younger materials with marly–arenaceous compositions, which allows it to more easily modify its course and riverbed, promoting significant fluvial dynamics. In contrast, the lands crossed by Bevano and Tenetra watercourses mainly consist of limestone, which is reflected in the higher stream slope and elevation, and in minor dynamism. For this reason, the available sediment depends on the amount of unstable material that can be identified from the updated geomorphological map. The two basins most susceptible to sediment production can be described as follows: in the Bevano basin, Quaternary debris is identified by the presence of inactive or dormant landslides, whereas in the Tenetra basin, a larger number of active landslides with clear signs of evolution are observed (most of them close to high values of IC).

4.8 Validation

The GIS analyses carried out in this work are based on a DTM created some years before the 2022 exceptional rainfall that profoundly affected the morphology of the territory with its consequences (landslides, linear and areal erosion along slopes, high solid transport in rivers, riverbank erosion). Therefore, the information deduced from the post-event observation and analysis was used to corroborate the spatial model's predictions and validate the methodology's reliability. Based on a comparison of pre- and post-rainfall events, it was possible to collect an archive with terrestrial and UAV photo documentation, the NDVI images, and highlighted control points on the field (Figs. 13 and 14).

A semi-quantitative remote analysis of the study area revealed morphological changes caused by the September 15 events and their spatial correlation with the results of this study. A difference analysis between two NDVI images (12 September and 18 September 2022; Fig. 13) highlighted a good correspondence

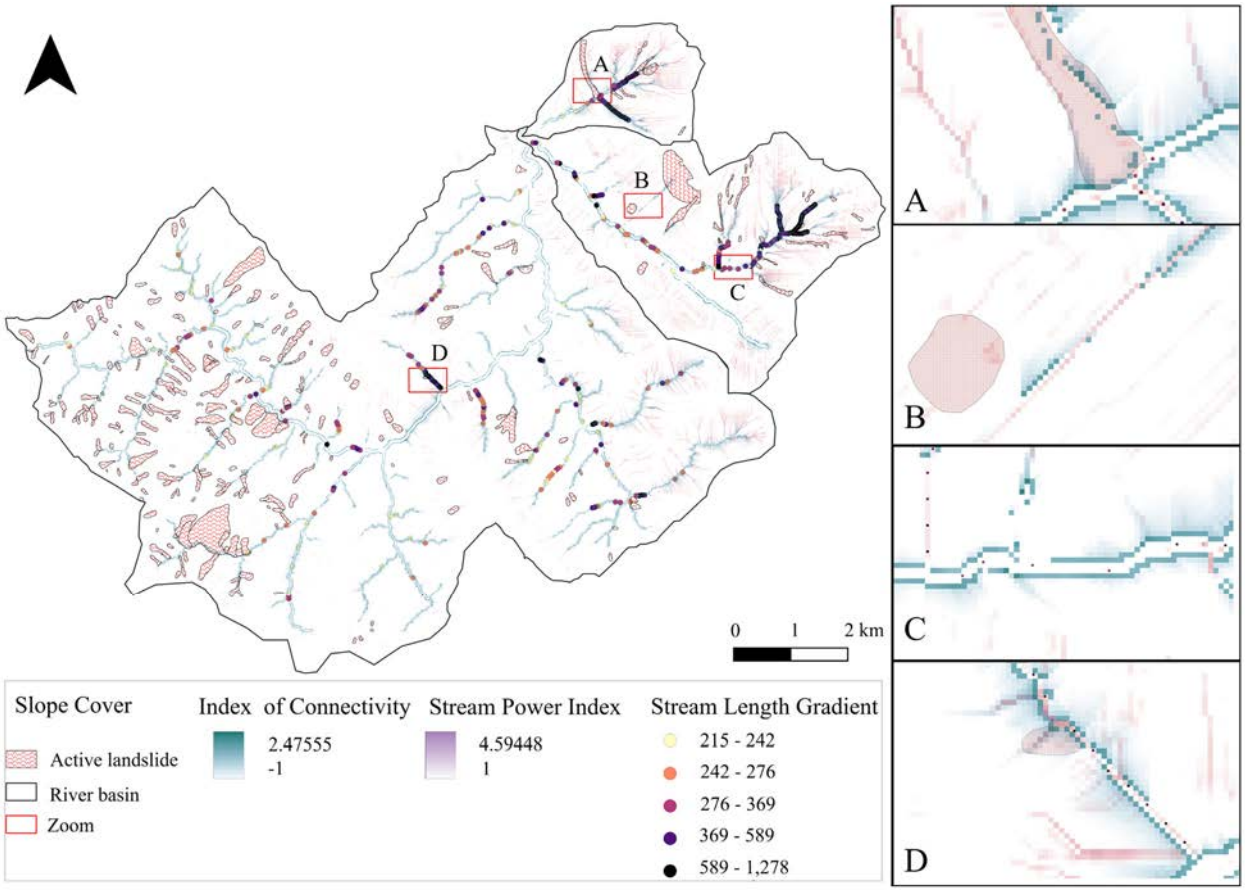

Fig. 12 Sediment availability map supported by fieldwork–sensitive values (IC and SPI), categorised to locate the highest values in the classes; V class of SL, isolated and classified in the quantile method in 5 classes.

between the results of the applied methodology and the actual case for the entire basin area in different geomorphologic contexts. The DEM of Difference (DoD) analysis illustrates a noticeable reduction in vegetation. Given that the two images were acquired only a few days apart, the observed changes can be reasonably attributed to the hydro-geomorphic event that occurred in September 2022. The decrease in vegetation is shown as a negative value on the pixel. Evaluating the number of pixels with negative signs highlights that the area affected is: 2.11 km^2 in the upper Burano River (3.1% of the total area), 0.44 km^2 in the Bevano Creek (2.8% of the total area), 0.13 km^2 in the Tenetra Creek (2.9% of the total area). The fieldwork included a series of general inspections carried out immediately after the event in September 2022 in collaboration with the Civil Protection Centre of the University of Florence and, subsequently, a lot of targeted examinations in the Bevano and Burano drainage areas in November 2023 and in the Tenetra basin in April 2024 (Fig. 14). The focus was on identifying the most sediment-producing areas, and in particular, the areas that may have caused damage to the basin and even to the city of Cantiano due to the merging of the three studied watercourses. UAV images were used to remotely localise the on-field control points. Based on a possible comparison of recently recorded information with the processing of older data, the fieldwork was carried out with extensive checking directly in the main areas identified as more mobilisable by the obtained maps.

Due to the territorial and environmental conditions, the hydraulic network reached very high flow levels in a very short time with a large transport of solid material, composed of debris with an average size of a few decimetres and plant material mobilised by the riverbeds themselves and the surrounding high slopes. The highly concentrated fluid overflowed at several points within wall levees or riverbanks and created anomalous, temporary transversal fluvial sections, sometimes causing the collapse of banks or embankment walls. One of these levee overtopping places was located exactly at the Burano's diversion bend into the tunnel (after overflowing upstream as well), as the raging water flows reclaimed the original riverbed that flooded up to the town centre. Concurrently, in the urban section of Bevano, the abruptly channelling waters broke their cover along two stretches, causing their waters to spread through the downtown streets from multiple sources. Even the sediment-laden waters from the steep valley of Tenetra came with very high energy, breaking a portion of the retaining wall just after the entombment (which resisted the power) and allowing further water runoff for the town. In the same catchment area, it is possible to observe an active landslide and its discharge of

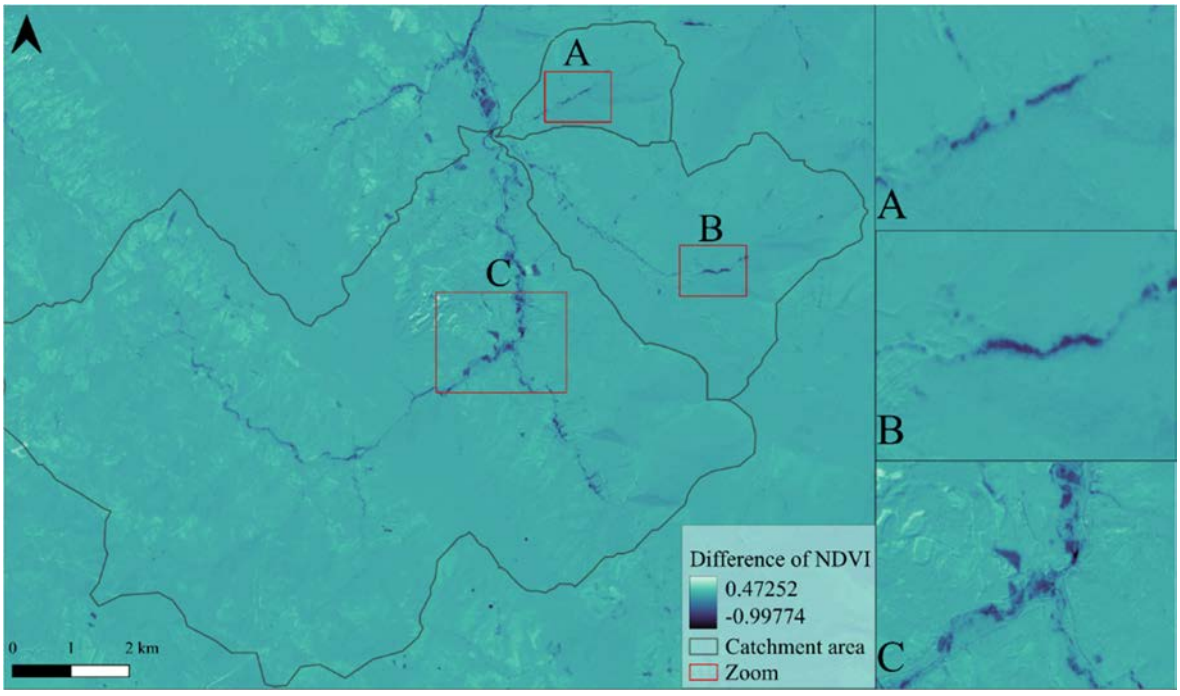

Fig. 13 NDVI – raster of difference of NDVI images – pre and post-flood event in Cantiano city – 12 September and 18 September. Image © 2022 Planet Labs PBC.

sediments into the floodplain of the Tenetra Creek (Fig. 14 - 2). In this river, whose discharge is not specified but could be estimated to be less than 1 m^3/s, a large deposit of highly heterogeneous debris has accumulated in the central part. Measured sizes ranging from 1.5/2 m in diameter to 0.01 m (Fig. 14 - 1). In some cases, as mentioned above, the sediments are sandier, allowing them to be transported further downstream. This is the case in the upper part of the Burano basin (Fig. 14 - 7-8) and a small part of its tributary, the Bevano. In the Bevano River, it has been observed that the increase in sediments in the riverbed mainly began following a major landslide on the right bank (Fig. 14 - 5). Severe and large mass movements were observed over the entire basin for validation. However, smaller events were also considered (Fig. 14 - 3). In the affected sites for which the surveys had suffered uncertainty in recognition, especially for the

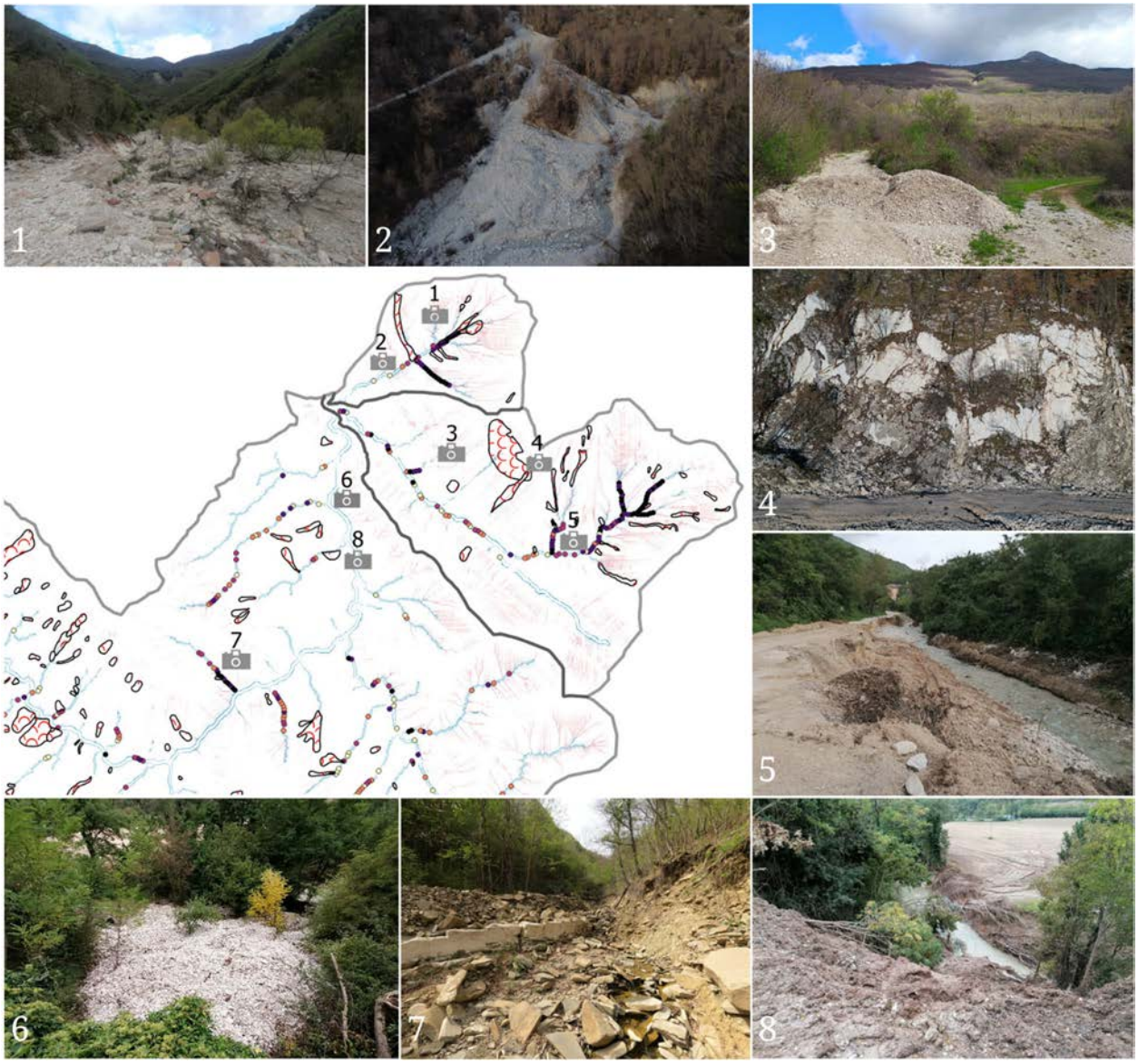

Fig. 14 The map highlights the surveyed sites, numbered according to the photographs taken in the field. All sediment sources were activated or reactivated during the September 2022 flood event. Field surveys were conducted in November 2023 and April 2024. 1) Central portion of Tenetra watercourse, post-flood riverbed; 2) Accumulation of debris transported and discharged in the Tenetra creek by a (very incised) lateral impluvium; 3) Small erosion channel with sediment accumulation in the downstream section of Bevano creek; 4) Landslide affecting the road along the saddle between the summits of Monte Acuto and Monte Catria; 5) Accumulation area of mainly terrigenous in the upstrem part of Bevano riverbed; 6) Erosion sector with calcareous debris discharge on the left bank of the Burano River; 7) Steep tributary of the Burano River, with coarse debris reaching the urbanised area; 8) Main reach of the Burano River with fine sediment accumulation in a lowland area.

smallest landslides, due to the vegetation cover and the steep slopes, the output maps helped to identify their location and their areal distribution and then confirm the robustness of the method's results.

5 Discussion

Recent literature provides a wide range of quantitative tools for investigating sediment connectivity, ranging from empirical or index-based approaches to physically based or cellular automata models. (Borselli et al. 2008; Cavalli et al. 2013; Coulthard et al. 2013; Heckmann et al. 2018). While these models can reproduce sediment fluxes with high accuracy (e.g., Morgan et al. 1998; Kirkby et al. 2008; Coulthard et al. 2013), they often rely on complex parameterisation and heterogeneous datasets, including rainfall erosivity, soil erodibility, and land use factors (Renard et al. 1997; Arnold et al. 2012; Panagos et al. 2015; Alewell et al. 2019). These data and parameter requirements often restrict model application in mountainous basins, where monitoring networks are sparse and rapid post-event evaluations are essential (Surian et al. 2020; Marchi et al. 2025).

This study addresses this limitation through a semi-quantitative, structurally based approach that integrates geomorphometric indices while reducing input data requirements and computational overhead, without compromising interpretative rigour. By synthesising geomorphometric parameters with expert geomorphological interpretation in a GIS environment, this method facilitates the rapid identification of sediment source areas and their degree of coupling with the drainage network. The integration of the SPI, IC, and SL indices enables the assessment of both the potential energy for sediment mobilisation and the structural pathways controlling transfer processes. Crucially, this geomorphometric assessment gains physical significance only when the indices are spatially combined with layers representing actual sediment sources, such as landslides or unconsolidated slope deposits. This finding highlights the fundamental importance of a robust geomorphological basis. The accurate characterisation of surface deposits is essential to anchor numerical models to the physical reality of the landscape, ensuring that the predicted connectivity reflects the actual availability of mobilisable material. Therefore, this combination bridges traditional morphometric analysis with a process-oriented understanding of sediment delivery, offering a flexible tool. With respect to the integrated HOTSED model (La Licata et al. 2025), which likewise focuses on the identification of sediment sources at the catchment scale, the approach presented here differs in both its structure and outputs. The workflow developed in this study can be performed within short computational times, relying solely on a digital terrain model, basic geological layers, and pre- and post-event landslide inventories. While the HOTSED framework primarily focuses on mapping and integrating potential sediment source areas with measures of structural and functional connectivity (e.g., GIS-based indices combining terrain and hydrological parameters), the approach proposed here further incorporates the Stream Length-Gradient (SL) index to explicitly account for variations in channel energy and sediment transport pathways that are not directly represented in the original HOTSED formulation. Although this approach shares a common objective with that of La Licata et al. (2025), which is to determine the areas that represent the source of material at the river basin level, they are structurally and computationally different. The HOTSED model calculates and combines indices that, when associated, define the relative physical potential for sediment transport from specific sources based on the new collection of geomorphic entities, while the method proposed here calculates three basic morphometric indices that together define the morphological setting influencing the sediment availability based on the pre-existing official databases. In addition, the HOTSED model combines mathematically the considered indices that represent: i) the potential of each geomorphic entity for being a source of sediment (PSS), ii) the inherent physical potential for sediment delivery from slopes (PST), and iii) the Structural Sediment Connectivity (STC). The model presented here calculates the following indices: i) the topographic potential flow erosion and its relationship to landscape processes in the entire basin (SPI), ii) the topographic variations along the river's path (SL), and iii) the index of connectivity (IC). This model does not consider the functional properties of the connectivity. Consequently, as concerns the final outputs, a single intuitive comprehensive raster is provided by the calculation of the HOTSED model; meanwhile, in this work, a synoptic raster map is generated that visually and spatially highlights the most critical values of the three calculated indices. In summary, although the proposed

workflow shares conceptual similarities with the approach of La Licata et al. (2025), it differs in several key aspects: (i) a simpler procedural structure; (ii) fewer input factors; (iii) a distinct erosion representation; (iv) the inclusion of a linear channel-based analysis; (v) heuristic rather than mathematical integration of outputs; and (vi) a multi-scale analytical framework, starting from the concept of the hydrographic basin and slope evaluation, the analysis then narrows to the hydrological system.

Analyses of sediment availability in morphogenetic processes are important, as they aim to identify specific areas that may represent sources of material potentially subject to mobilisation (Batista et al. 2022; Shi et al. 2025). From this perspective, the derived geomorphological map (Fig. 7 enabled the identification of slope and fluvial-margin deposits, facilitating an initial assessment of sediment availability within the study area. In an attempt to isolate the most prone to sediment production areas, slope movements retrieved from the national landslide database showing signs of ongoing evolution were considered. However, sediment availability alone does not imply effective mobilisation, which also depends on the hydrodynamic and topographic conditions capable of entraining and transporting material. From the SPI map (Fig. 8), slope sectors where flow energy increases were therefore identified, indicating an enhanced potential for the entrainment of material from both hillslope deposits and channel sediments. To further evaluate whether mobilised sediments can be effectively transferred from source areas to the fluvial network, sediment connectivity was subsequently assessed at the basin scale using the IC index. The IC map (Fig. 9) provided an expedient means of assessing sediment dynamics, graphically illustrating the potential for sediment to enter the river system and indirectly indicating the location of source areas. While several studies conducted in mountain basins incorporate land-use parameters (Borselli et al. 2008; Zingaro et al. 2019; Zhao et al. 2020; Michalek et al. 2021; Guo et al. 2023; Abebe et al. 2023), this factor may be limiting in morphologically complex settings. Accordingly, in this study, the roughness parameter proposed by Cavalli et al. 2013 was adopted, as it is better suited to environments characterised by steep slopes and marked lithological heterogeneity. Furthermore, land use in the study area is relatively homogeneous. In order to investigate how these sediment transfer processes are reflected in the longitudinal organisation of the channel network, a stream-profile analysis was subsequently carried out using the Stream Length–Gradient (SL) index. The SL index map (Fig. 10) identified knickpoints along the stream profiles, highlighting clusters of values associated with sharp changes in hydraulic gradient. The spatial distribution of anomalies along the drainage network was emphasised using a five-class quantile classification. To refine and validate the interpretation provided by the SL index, a traditional analysis of longitudinal river profiles was additionally performed. This approach (Fig. 11) supported the interpretation of the SL index results by better characterising the geometric nature of the identified morphological discontinuities - particularly in site-specific cases - and by distinguishing between anthropogenically induced and naturally driven profile anomalies. This allowed the identification of channel reaches where interactions between hillslope and fluvial processes are most likely to occur. Therefore, the LS index was used to objectively identify longitudinal gradient anomalies at the basin scale, while traditional longitudinal profile analysis provided a detailed geometric interpretation of these features, allowing their origin to be more reliably assessed. The combined use of both approaches reduces interpretative redundancy and strengthens the robustness of knickpoint detection.

The final sediment availability map (Fig. 12) highlights slope sectors characterised by the highest sediment production, enabling the identification of areas with high susceptibility to rapid evolution along the slope. Therefore, the map should not be interpreted strictly as a simple depiction of sediment presence, but rather as a more articulated, process-oriented representation identifying where sediment can be effectively mobilised and transferred toward the fluvial system. The robustness of the results and of the adopted methodology was assessed through comparison with the documented geomorphological effects of the 2022 rainfall event, showing that sediment mobilisation was concentrated in areas identified by the pre-event DTM analysis. The validation phase demonstrated a strong spatial correlation between high-index zones and the location and geometry of occurred landslides, as reported in the E-LIM inventory.

During this reference event, the upper part of the Tenetra basin had a strong mobilisation due to the high availability of sediment, steep slopes and low drainage

density, showing a very effective relation between the high values of connectivity and high transit of material. On the contrary, in the upper Bevano basin, the low sediment availability made almost ineffective the material movement thanks to lower values of connectivity, which, however, led the flows to increase at the foot of the slope, creating a strong erosion zone on the main channel with a bridge collapse. The areas with the highest productivity and likelihood of flowing into the river network are mainly represented by secondary tributaries and small, steep ditches. Three main sectors can be distinguished (Figs. 12-14): (i) the Tenetra basin, where land-cover changes affected approximately 2.9% of the total area; (ii) the transitional zone between the Tenetra and Bevano basins, characterised by the occurrence of multiple rapid landslides; and (iii) the upper Burano basin, particularly its higher-order tributaries, which mobilised fine sediments along the fluvial network, ultimately transporting mud to the town of Cantiano. All these characteristics are reflected in the generated map. Nevertheless, the area exhibiting the greatest propensity for sediment discharge in the final map is the Tenetra basin, located approximately 1 km upstream from its confluence with the Burano River.

The results suggest that, particularly during short-duration, high-intensity rainfall events such as that of September 2022, terrain-based connectivity indices such as the IC (Cavalli et al. 2013), combined with geomorphic indices including SPI and SL, are effective in identifying areas prone to sediment mobilisation. When interpreted together with topographic discontinuities (e.g., slope breaks and knickzones), these indices provide a more robust representation of sediment source activation than approaches based solely on independent DTM-derived metrics (e.g., Heckmann et al. 2018; Zingaro et al. 2019; Cavalli et al. 2021; Torresani et al. 2023).

6 Conclusions

Investigating hillslope–channel coupling is essential for understanding sediment production and transfer across mountainous catchments. This study contributes to refining the methodologies used to assess erosion and sediment movement processes in such geomorphological settings. The work also aligns with current international initiatives dedicated to sediment management, ultimately supporting the development of decision-support frameworks for sustainable sediment governance and for geo-hydrological risk management. The study area, in which the method was developed, is located in the Northern Apennines (Italy), and in particular in a mountainous hydrographic basin including three sub-basins, different by their geological and geomorphological characteristics. These areas were affected by an extreme rainfall event in September 2022, which had a significant impact on landforms as well as on human structures and infrastructures. A progressive workflow is proposed, beginning with hydro-geomorphological characterisation and followed by GIS-based analyses aimed at identifying sediment sources, stream power, catchment-scale connectivity, and longitudinal channel anomalies. Although this approach shares the overarching objective of existing methodologies, it differs substantially in both structural design and computational framework. The proposed method was applied using geospatial data available before the 2022 event, and its results were subsequently validated by observing the geomorphological changes induced by the above-mentioned extreme rainfall event. Validation was performed through multi-source comparison, integrating NDVI analysis, UAV photogrammetry, and detailed traditional field surveys. The workflow computes several morphometric indices and generates their corresponding raster maps. These outputs are integrated into a final sediment availability map, which delineates the most susceptible areas by identifying the convergence of critical values across the used data. The sediment availability map provides a hazard-oriented synthesis of basin-scale sediment dynamics by identifying slope sectors and channel reaches where sediment sources, mobilisation potential, and transfer efficiency coincide, thereby delineating areas prone to rapid and potentially hazardous geomorphic responses. In particular, by integrating geomorphological evidence, SPI-derived flow energy, roughness-based sediment connectivity (IC), and longitudinal channel controls identified through the SL index and traditional longitudinal profile analyses, the map highlights zones of strong hillslope–channel coupling that are especially susceptible to sediment mobilisation and downstream propagation during short-duration, high-intensity rainfall events. The strong spatial correspondence between high-index areas and the landslides documented following the 2022 rainfall event confirms

that the map effectively captures the pre-event conditions governing sediment release and transfer, supporting its use as a tool for prioritising monitoring, early-warning strategies, and targeted mitigation measures in geomorphically sensitive catchments. Overall, the proposed framework offers a scalable methodology with intuitive outputs that can be used to forecast landscape evolution, even under extreme rainfall conditions.

While the proposed workflow demonstrates robust operational performance using freely accessible datasets, its precision could be further enhanced through higher-quality input data. In particular, the integration of high-resolution datasets would likely improve the accuracy of the geomorphological outputs. Looking ahead, there is potential to implement and consolidate the full processing chain as a standalone automated framework, seamlessly merging geomorphological analysis with functional connectivity metrics.

Acknowledgments

This study was conducted within the framework of a PhD project developed at the University of Urbino and supported by the Italian Ministry of University and Research (MUR) under the National Recovery and Resilience Plan (PNRR). The authors gratefully acknowledge this institutional support, which enabled the initial development of the research. No external funding from private entities was received.

Author Contributions

GUIDI Erica: Conceptualisation; data curation; methodology; software development; data processing; preparation of the original draft; MORELLI Stefano: Conceptualisation; investigation; manuscript review and editing; PAPPAFICO Giulio Fabrizio: Data collection; data processing; cartographic and graphical production; manuscript review and editing; CONFUORTO Pierluigi: Data validation; manuscript review and editing.

Ethics Declaration

Availability of Data/Materials: The datasets generated during this study are available from the corresponding author upon reasonable request and within the framework of cooperation agreements and scientific research projects.

Conflict of Interest: The authors declare no conflict of interest.

Open Access

Funding note: Open access funding provided by Università degli Studi di Urbino Carlo Bo within the CRUI-CARE Agreement.

References

Abebe N, Eekhout J, Vermeulen B, et al. (2023) The potential and challenges of the 'RUSLE-IC-SDR' approach to identify sediment dynamics in a Mediterranean catchment. Catena 233:107480. https://doi.org/10.1016/j.catena.2023.107480

Abu El-Magd SO, Orabi HO, Ali SA, et al. (2021) An integrated approach for evaluating the flash flood risk and potential erosion using the hydrologic indices and morpho-tectonic parameters. Environ Earth Sci 80:694. https://doi.org/10.1007/s12665-021-10013-0

Alewell C, Borrelli P, Meusburger K, et al. (2019) Using the USLE: Chances, challenges and limitations of soil erosion modelling. Int. Soil Water Conserv Res 7(3): 203-225. https://doi.org/10.1016/j.iswcr.2019.05.004

Amici M, Spina R (2002) Mean annual and seasonal precipitation over the Marche region for the period 1950-2000. Marche Region Civil Protection, Center for Ecology and Climatology, Macerata Experimental Geophysical Observatory. (In Italian)

Arnold JG, Moriasi DN, Gassman PW, et al. (2012) SWAT: Model use, calibration, and validation. Trans. ASABE 55(4):1491-1508. https://doi.org/10.13031/2013.42256

Barchi MR, Alvarez W, Shimabukuro DH (2012) The Umbria-Marche Apennines as a double orogen: Observations and hypotheses. Ital J Geosci 131:258-271. https://doi.org/10.3301/IJG.2012.17

Batista PVG, Fiener P, Scheper S, et al. (2022) A conceptual model-based sediment connectivity assessment for patchy agricultural catchments. Hydrol Earth Syst Sci 26:3753-3770. https://doi.org/10.5194/hess-26-3753-2022

Borselli L, Cassi P, Torri D (2008) Prolegomena to sediment and flow connectivity in the landscape: A GIS and field numerical assessment. Catena 75:268-277. https://doi.org/10.1016/j.catena.2008.07.006

Bracken LJ, Turnbull L, Wainwright J, et al. (2015) Sediment connectivity: a framework for understanding sediment transfer at multiple scales. Earth Surf Process Landf 40(2):177-188. https://doi.org/10.1002/esp.3635

Brenna A, Scorpio V, Finotello A, et al. (2025) Suspended transport of gravel in rivers: Empirical evidence from the 2022 flood in the Misa River (Eastern Apennines, Italy). Earth Surf Process Landf 50(6): e70081. https://doi.org/10.1002/esp.70081

Brierley G, Fryirs K, Jain V (2006) Landscape Connectivity: The Geographic Basis of Geomorphic Applications. Area 38(2):165-174. https://www.jstor.org/stable/20004523

Campobasso C, Carton A, Chelli A, et al. (2021) Carg Project: changes and additions to notebook N. 4/1994. Notebooks, Series III, 13(1): Version 2.0. (In Italian)

Cavalli M, Trevisani S, Comiti F, Marchi L (2013) Geomorphometric assessment of spatial sediment connectivity in small Alpine catchments. Geomorphology 188:31-41. https://doi.org/10.1016/j.geomorph.2012.05.007

Cavalli M, Crema S, Borselli L, et al. (2021) Sediment connectivity assessment through a geomorphometric approach review of recent applications, The CNR IRPI's contribution to the country's system for mitigating geohydrological risks, Rome, 25-26/11/2021. http://www.cnr.it/prodotto/i/460042

Chowdhury MdS (2023) Modelling hydrological factors from DEM using GIS. MethodsX 10:102062. https://doi.org/10.1016/j.mex.2023.102062

Confuorto P, Franceschini R, Scarpitta L, et al. (2025) Event-based landslide inventory through very high-resolution optical images and field surveys. Geoenviron. Disasters 12:23. https://doi.org/10.1186/s40677-025-00328-6

Corti M, Francioni M, Abbate A, et al. (2024) Analysis and modelling of the september 2022 flooding event in the Misa basin. Ital J Eng Geol Environ 1:69-76. https://doi.org/10.4408/IJEGE.2024-01.S-08

Cossart É, Fressard M (2017) Assessment of structural sediment connectivity within catchments: insights from graph theory. Earth Surf Dynam 5:253-268. https://doi.org/10.5194/esurf-5-253-2017

Coulthard TJ, Neal JC, Bates PD, et al. (2013) Integrating the LISFLOOD-FP 2D hydrodynamic model with the CAESAR model: implications for modelling landscape evolution. Earth Surf Process Landf 38:1897-1906. https://doi.org/10.1002/esp.3478

Crema S, Cavalli M (2018) SedInConnect: a stand-alone, free and open source tool for the assessment of sediment connectivity. Comput Geosci 111:39-45. https://doi.org/10.1016/j.cageo.2017.10.009

Donnini M, Santangelo M, Gariano SL, et al. (2023) Landslides triggered by an extraordinary rainfall event in Central Italy on September 15, 2022. Landslides 20(10):2199-2211. https://doi.org/10.1007/s10346-023-02109-4

Fryirs KA (2013) (Dis)Connectivity in catchment sediment cascades: a fresh look at the sediment delivery problem. Earth Surf Process Landf 38:30-46. https://doi.org/10.1002/esp.3242

Fryirs KA (2017) River sensitivity: a lost foundation concept in fluvial geomorphology. Earth Surf Process Landf 42:55-70. https://doi.org/10.1002/esp.3940

Gentilucci M, Materazzi M, Pambianchi G, et al. (2020) Temperature variations in Central Italy (Marche region) and effects on wine grape production. Theor Appl Climatol 140(1-2):303-312. https://doi.org/10.1007/s00704-020-03089-4

Guo Z, Wu L, Liu S, et al. (2023) An integrated watershed modelling framework to explore the covariation between sediment connectivity and soil erosion. Eur J Soil Sci 74(5): e13412. https://doi.org/10.1111/ejss.13412

Hack JT (1973) Stream-profile analysis and stream-gradient index. J Res U.S. Geol Surv 1(4):421-429. https://pubs.usgs.gov/publication/70161653 (accessed 30 July 2024)

Harvey AM (2001) Coupling between hillslopes and channels in upland fluvial systems: implications for landscape sensitivity, illustrated from the Howgill Fells, northwest England. Catena 42(2):225-50. https://doi.org/10.1016/S0341-8162(00)00139-9

Heckmann T, Cavalli M, Cerdan O, et al. (2018) Indices of sediment connectivity: opportunities, challenges and limitations. Earth Sci Rev 187:77-108. https://doi.org/10.1016/j.earscirev.2018.08.004

Hooke J (2003) Coarse sediment connectivity in river channel systems: a conceptual framework and methodology. Geomorphology 56(1-2):79-94. https://doi.org/10.1016/S0169-555X(03)00047-3

Hooke J, Souza J (2021) Challenges of mapping, modelling and quantifying sediment connectivity. Earth-Sci Rev 223:103847. https://doi.org/10.1016/j.earscirev.2021.103847

Horton RE (1932) Drainage basin characteristics. Trans. Am. Geophys. Union 13:350-361.

Horton RE (1945) Erosional development of streams and their drainage basins; hydrophysical approach to quantitative morphology. Bull Geol Soc Am 56:275-370.

Hungr O, Leroueil S, Picarelli L (2014) The Varnes classification of landslide types, an update. Landslides 11:167-194. https://doi.org/10.1007/s10346-013-0436-y

ISPRA - Italian Institute for Environmental Protection and Research (2019) CORINE Land Cover Italia 2018 [Data set]. https://www.isprambiente.gov.it/it/attivita/suolo-e-territorio/suolo/copertura-del-suolo/corine-land-cover (In Italian, accessed on 31 December 2025)

Kemp DB, Sadler PM, Vanacker V (2020) The human impact on North American erosion, sediment transfer, and storage in a geologic context. Nat Commun 11:6012. https://doi.org/10.1038/s41467-020-19744-3

Kirkby MJ, Irvine BJ, Jones RJA, et al. (2008) The PESERA coarse scale (1 km) regional soil erosion model for Europe: first results. Eur J Soil Sci 59(4) : 676-686. https://doi.org/10.1111/j.1365-2389.2008.01072.x

Köppen W (1936) The geographical system of climates. In: Köppen W, Geiger R (eds.), Handbook of Climatology. Gebrüder Borntraeger, Berlin. pp 1-44. (In German)

Koreňová S, Michalková MŠ, Máčka Z, et al. (2024) Linking sediment connectivity with sediment transport risk assessment in small forested catchments in the Czech Republic. River Res Appl 40(7):1343-1362. https://doi.org/10.1002/rra.4295

La Licata M, Bosino A, Sadeghi SH, et al. (2025) HOTSED: A new integrated model for assessing potential hotspots of sediment sources and related sediment dynamics at watershed scale. Int Soil Water Conserv Res 13(1):80-101. https://doi.org/10.1016/j.iswcr.2024.06.002

Latini I (2018) Floristic-vegetational analysis and the changes of biodiversity in the moist environments of Metauro river's final stretch. Unpublished thesis. Polytechnic University of Marche (Italy).

Liu C, Walling DE, He Y (2018) The International Sediment Initiative case studies of sediment problems in river basins and their management. Int J Sediment Res 33(2):216-219. https://doi.org/10.1016/j.ijsrc.2017.05.005

Marchi M, Bertolini I, Tonni L, et al. (2025) An Extensive Italian Database of River Embankment Breaches and Damages. Water

17(15):2202.
https://doi.org/10.3390/w17152202
Martini L, Cavalli M, Picco L (2022) Predicting sediment connectivity in a mountain basin: a quantitative analysis of the Index of Connectivity. Earth Surf Process Landf 47(6):1500-1513.
https://doi.org/10.1002/esp.5331
Messenzehl K, Hoffmann T, Dikau R (2014) Sediment connectivity in the high-alpine valley of Val Müschauns, Swiss National Park—linking geomorphic field mapping with geomorphometric modelling. Geomorphology 221:215-229.
https://doi.org/10.1016/j.geomorph.2014.05.033
Michalek A, Zarnaghsh A, Husic A (2021) Modeling linkages between erosion and connectivity in an urbanizing landscape. Sci Total Environ 764:144255.
https://doi.org/10.1016/j.scitotenv.2020.144255
Miller VC (1953) A quantitative geomorphic study of drainage basin characteristics in the clinch mountain area. Virgina and Tennessee, Proj. NR 389-402, Technical report 3, Columbia University, Department of Geology, ONR, New York.
Mishra K, Sinha R, Jain V, et al. (2019) Towards the assessment of sediment connectivity in a large Himalayan River basin. Sci Total Environ 661:251-265.
https://doi.org/10.1016/j.scitotenv.2019.01.118
Moore ID, Grayson RB, Ladson AR (1991) Digital terrain modelling: A review of hydrological, geomorphological, and biological applications. Hydrol Process 5:3-30.
https://doi.org/10.1002/hyp.3360050103
Moosdorf N, Cohen S, Hagke C (2018) A global erodibility index to represent sediment production potential of different rock types. Appl Geogr 101:36-44.
https://doi.org/10.1016/j.apgeog.2018.10.010
Morelli S, Bonì R, Guidi E, et al. (2023) The flood in the Marche region of September 15, 2022: causes and consequences. In: Cencetti C, Di Matteo L (eds.), Fluvial Dynamics. River Knowledge for Planning and Land Protection. Cult Territ Linguaggi 24:136-147. ISBN 9788894469783. (In Italian)
http://www.ctl.unipg.it/issues/CTL_24.pdf
Morgan RPC, Quinton JN, Smith RE, et al. (1998) The European Soil Erosion Model (EUROSEM): a dynamic approach for predicting sediment transport from fields and small catchments. Earth Surf Process Landf 23(6):527-544.
https://doi.org/10.1002/(SICI)1096-9837(199806)23:6<527::AID-ESP868>3.0.CO;2-5
Najafi S, Sadeghi SH, Heckmann T (2021a) Analysis of sediment accessibility and availability concepts based on sediment connectivity throughout a watershed. Land Degrad Dev 32: 3023-3044.
https://doi.org/10.1002/ldr.3964
Najafi S, Dragovich D, Heckmann T, et al. (2021b) Sediment connectivity concepts and approaches. Catena 196: 104880.
https://doi.org/10.1016/j.catena.2020.104880
Nanni T, Vivalda PM (2009) Hydrogeology of the carbonate, terrigenous and alluvial aquifers between the Cesano and Potenza rivers (Central Marche). GNDCI-CNR, Unità Operativa 10. ISBN 9788890455414. (In Italian)
https://doi.org/10.13140/2.1.3450.6883
Panagos P, Borrelli P, Poesen J, et al. (2015) The new assessment of soil loss by water erosion in Europe. Environ Sci Policy 54: 438-447.
https://doi.org/10.1016/j.envsci.2015.08.012
Parsons AJ, Bracken L, Poeppl RE, et al. (2015) Introduction to special issue on connectivity in water and sediment dynamics. Earth Surf Process Landf 40(9): 1275-1277.
https://doi.org/10.1002/esp.3714
Pérez-Peña JV, Azañón JM, Azor A, et al. (2009) Spatial analysis of stream power using GIS: SLk anomaly maps. Earth Surf Process Landf 34:16-25.
https://doi.org/10.1002/esp.1684
Piacentini D, Troiani F, Marini M, et al. (2020) GIS-based geomorphometric analysis of stream networks in mountainous catchments. Implications for slope stability. In: Alvioli M, Marchesini I, Melelli L, Guth P (eds.), Proceedings of the Geomorphometry 2020 Conference. Perugia, Italy, CNR Edizioni 270:254-257.
https://doi.org/10.30437/GEOMORPHOMETRY2020_68
Planet Team (2022) Planet Application Program Interface: In Space for Life on Earth. San Francisco, CA.
Poeppl RE, Polvi LE, Turnbull L (2023) (Dis)connectivity in hydro-geomorphic systems - emerging concepts and their applications. Earth Surf Process Landf 48:1089-1094.
https://doi.org/10.1002/esp.5574
Raphael A, Ngaga Y, Lalika M (2023) Watershed degradation and water provision in Morogoro Municipality, Tanzania. Ecohydrol Hydrobiol 23(2):272-279.
https://doi.org/10.1016/j.ecohyd.2022.12.004
Regione Marche (2022) SIRMIP - Weather-Hydro-Pluviometric Regional Information System. (In Italian)
http://app.protezionecivile.marche.it/sol/indexjs.sol?lang=it (Accessed on 12 July 2024)
Renard KG (1997) Predicting soil erosion by water: a guide to conservation planning with the Revised Universal Soil Loss Equation (RUSLE). US Department of Agriculture, Agricultural Research Service. Agriculture Handbook 703.
Sadeghi SH, Najafi S, Bakhtiari AR (2017) Sediment contribution from different geologic formations and land uses in an Iranian small watershed, case study. Int J Sediment Res 32:210-220.
https://doi.org/10.1016/j.ijsrc.2017.02.002
Santangelo M, Althuwaynee O, Alvioli M, et al. (2023) Inventory of landslides triggered by an extreme rainfall event in Marche-Umbria, Italy, on 15 September 2022. Sci. Data 10(1):427.
https://doi.org/10.1038/s41597-023-02336-3
Schumm SA (1956) Evolution of drainage systems and slopes in badlands at Perth Amboy, New Jersey GSA Bull 67(5):597-646.
https://doi.org/10.1130/0016-7606(1956)67[597:EODSAS]2.0.CO;2
Scisciani V (2009) Styles of positive inversion tectonics in the Central Apennines and in the Adriatic foreland: Implications for the evolution of the Apennine chain (Italy). J Struct Geol 31: 1276-1294.
https://doi.org/10.1016/j.jsg.2009.02.004
Senatore A, Furnari L, Nikravesh G, et al. (2025) Increasing Daily Extreme and Declining Annual Precipitation in Southern Europe: A Modeling Study on the Effects of Mediterranean Warming, EGUsphere [preprint].
https://doi.org/10.5194/egusphere-2025-1567
Shekar PR, Mathew A (2022) Morphometric analysis for prioritizing sub-watersheds of Murredu River basin, Telangana State, India, using a geographical information system. J Eng Appl Sci 69: 44.
https://doi.org/10.1186/s44147-022-00094-4
Shekar PR, Mathew A (2024) Morphometric analysis of watersheds: A comprehensive review of data sources, quality, and geospatial techniques. Watershed Ecol Environ 6:13-25.
https://doi.org/10.1016/j.wsee.2023.12.001
Shi C, Liang Y, Qin W, et al. (2025) Review of sediment connectivity: Conceptual connotations, characterization indicators, and their relationships with soil erosion and sediment yield. Earth-Sci Rev 264:105091.
https://doi.org/10.1016/j.earscirev.2025.105091
Soldini L, Darvini G (2025) Variation in the Extreme Temperatures and Related Climate Indices for the Marche Region, Italy. Climate 13(3): 58.
https://doi.org/10.3390/cli13030058
Sreedevi PD, Subrahmanyam K, Ahmed S (2005) The significance of morphometric analysis for obtaining groundwater potential zones in a structurally controlled terrain. Environ Geol 47: 412-420.
https://doi.org/10.1007/s00254-004-1166-1
Strahler AN (1964) Quantitative Geomorphology of Drainage Basins and Channel Networks. In: Chow V (ed.), Handbook of Applied Hydrology. McGraw Hill, NewYork. pp 439-476.
Summerfield MA (1991) Global Geomorphology. An Introduction to the Study of Landforms. Prentice Hall, Pearson Education

Ltd., Harlow, UK.
Surian N, Brenna A, Borga M, et al. (2020) Flood hazard in mountain streams: the key role of geomorphic processes during high magnitude events. In EGU General Assembly 2020, EGU2020-9682. https://doi.org/10.5194/egusphere-egu2020-9682
Syvitski JPM, Vörösmarty CJ, Kettner AJ, et al. (2005) Impact of humans on the flux of terrestrial sediment to the global coastal ocean. Science 308(5720):376-380. https://doi.org/10.1126/science.1109454
Tarquini S, Isola I, Favalli M, et al. (2007) TINITALY/01: a new Triangular Irregular Network of Italy. Ann Geophys 50(3): 407-425. https://doi.org/10.4401/ag-4424
Tarquini S, Nannipieri L (2017) The 10 m-resolution TINITALY DEM as a trans-disciplinary basis for the analysis of the Italian territory: Current trends and new perspectives. Geomorphology 281: 108-115. https://doi.org/10.1016/j.geomorph.2016.12.022
Tarquini S, Isola I, Favalli M, et al. (2023) TINITALY, a digital elevation model of Italy with a 10 meters cell size (Version 1.1). National Institute of Geophysics and Volcanology (INGV). https://doi.org/10.13127/tinitaly/1.1
Torresani L, Piton G, D'Agostino V (2023) Morphodynamics and sediment connectivity index in an unmanaged, debris-flow prone catchment: a through-time perspective. J Mt Sci 20(4):891-910. https://doi.org/10.1007/s11629-022-7746-2
Trigila A, Iadanza C, Guerrieri L (2007) The IFFI Project (Italian Landslide Inventory): Methodology and Results. Proceedings 772 of the Guidelines for Mapping Areas at Risk of Landslides in Europe; Javier Hervás: Ispra, Italy, October 23, 2007. 773:60.
Trigila A, Iadanza C (2008) Landslides in Italy, Special Report. Italian National Institute for Environmental Protection and Re-774 search-Geological Survey of Italy/Land Protection and Georesources Department, Rome, Italy.
Trigila A, Iadanza C, Spizzichino D (2010) Quality Assessment of the Italian Landslide Inventory Using GIS Processing. Landslides 7: 455-470. https://doi.org/10.1007/s10346-010-0213-0
Troiani F, Galve JP, Piacentini D, et al. (2014) Spatial analysis of stream length-gradient (*SL*) index for detecting hillslope processes: A case of the Gállego River headwaters (Central Pyrenees, Spain). Geomorphology 214: 183-197. https://doi.org/10.1016/j.geomorph.2014.02.004
Turnbull L, Hütt MT, Ioannides AA, et al. (2018) Connectivity and complex systems: learning from a multi-disciplinary perspective. Appl Netw Sci 3: 1-49. https://doi.org/10.1007/s41109-018-0067-2
UNESCO (2022) IHP-IX: strategic plan of the intergovernmental hydrological programme: science for a water secure world in a changing environment, ninth phase 2022-2029. UNESCO, Paris. p 51. https://unesdoc.unesco.org/ark:/48223/pf0000381318 (accessed 30 July 2024)
Wainwright J, Turnbull L, Ibrahim TG, et al. (2011) Linking environmental regimes, space and time: Interpretations of structural and functional connectivity. Geomorphology 126(3-4):387-404. https://doi.org/10.1016/j.geomorph.2010.07.027
Wilson JP (2012) Digital Terrain Model. Geomorphology 137(1):107-121. https://doi.org/10.1016/j.geomorph.2011.03.012
Wohl E (2017) Connectivity in rivers. Prog Phys Geogr 41(3):345-362. https://doi.org/10.1177/0309133317714972
Wohl E, Brierley G, Cadol D, et al. (2019) Connectivity as an emergent property of geomorphic systems. Earth Surf Process Landf 44: 4-26. https://doi.org/10.1002/esp.4434
Zanandrea F, Michel GP, Kobiyama M, et al. (2021) Spatial-temporal assessment of water and sediment connectivity through a modified connectivity index in a subtropical mountainous catchment. Catena 204:105380. https://doi.org/10.1016/j.catena.2021.105380
Zhao G, Gao P, Tian P, et al. (2020) Assessing sediment connectivity and soil erosion by water in a representative catchment on the Loess Plateau, China. Catena 185:104284 https://doi.org/10.1016/j.catena.2019.104284
Zingaro M, Refice A, Giachetta E, et al. (2019) Sediment mobility and connectivity in a catchment: A new mapping approach. Sci Total Environ 672:763-775. https://doi.org/10.1016/j.scitotenv.2019.03.461